# Comparison and validation of force fields for deep eutectic solvents in combination with water and alcohol dehydrogenase

Jan Philipp Bittner,[a] Lei Huang,[b] Ningning Zhang,[b] Selin Kara,[b] Sven Jakobtorweihen,[a,c]*

(a) Institute of Thermal Separation Processes, Hamburg University of Technology, Eißendorfer Straße 38, Hamburg, Germany, 21073

(b) Department of Biological and Chemical Engineering, Biocatalysis and Bioprocessing Group, Aarhus University, Gustav Wieds Vej 10, Aarhus, Denmark, 8000

(c) Department for Chemical Reaction Engineering, Hamburg University of Technology, Eißendorfer Straße 38, Hamburg, Germany, 21073

*Alcohol dehydrogenase, deep eutectic solvents, force fields, molecular dynamics simulations, periodic perturbation method*

**ABSTRACT:** Deep eutectic solvents (DESs) have become popular as environmental-friendly solvents for biocatalysis. Molecular dynamics (MD) simulations offer an in-depth analysis of enzymes in DESs, but their performance depends on the force field chosen. Here we present a comprehensive validation of three bio-molecular force fields (CHARMM, Amber and OPLS) for simulations of alcohol dehydrogenase (ADH) in DESs composed of choline chloride and glycerol/ethylene glycol with varying water content. Different properties (e.g., protein structure and flexibility, solvation layer, H-bonds) were used for validation. For two properties (viscosity and water activity) also experiments were performed. The viscosity was calculated with the periodic perturbation method, whereby its parameter dependency is disclosed. A modification of Amber was identified as best performing model for low water contents, whereas CHARMM outperforms the other models at larger water concentrations. An analysis of ADH's structure and interactions with the DESs revealed similar predictions for Amber and CHARMM.

## INTRODUCTION

The usage of enzymes for the development of greener and sustainable alternatives for synthesis routes has become a key factor in the chemical industry.[1] The choice of the solvent plays thereby a central role in developing future biocatalytic applications. In the past years, deep eutectic solvents (DESs) have emerged as a new solvent class for biocatalysis[2–8] and have been labeled as the 'solvent of the 21st century'.[9] The DESs, as first described by Abbot et al.,[10] can be formed by mixing a quaternary ammonium salt (e.g., choline chloride (ChCl)), acting as a hydrogen bond acceptor (HBA), with a hydrogen bond donor (HBD, e.g., glycerol, urea). It has to be stated that the presence of hydrogen bonding alone is not a sufficient definition for a DES.[11] In order for the DES to be called a "deep" eutectic the eutectic point of the mixture has to be considerably lower than the eutectic of an ideal solution[11] (e.g., $\Delta T \approx 40$K for ChCl-Gly[12]), which is caused by strong attractive interactions between the two DES components. This non-ideality of DESs is a key feature for biocatalysis, as it widens the range of accessible solvents,[3,13,14] that are solid as pure components, and can lead to a lower availability of the DES constituents as a reaction partner.[15] As deep eutectic solvents can be tailored from natural components, they meet the requirements of sustainable and environmental-friendly solvent alternatives for biochemical reactions.

A popular group of sustainable DESs is based on choline chloride as HBA. Commercial names were assigned to these mixtures according to their HBD for example, glyceline (glycerol), reline (urea) or ethaline (ethylene glycol). However, this nomenclature can lead to the false impression, that the formation of a DES led to a creation of a new substance. Unlike ionic liquids (ILs), deep eutectic solvents are neither new substances nor any kind of pseudo-components; instead they are simply binary mixtures.[11] Hence, here we use the common convention of labelling the DESs by its constituents, that are ChCl-Gly (choline chloride : glycerol (molar ratio 1:2)) and ChCl-EG (choline chloride : ethylene glycol (molar ratio 1:2)) rather than using the commercial names (glyceline and ethaline).

Molecular dynamics (MD) simulations represent a vital tool to gain deep insights into the behavior of enzymes in a DES environment. In conjunction with experimental investigations, they can offer a comprehensive perspective on the enzyme catalysis and can help to guide the selection of solvents for biocatalytic applications. However, the choice of the interaction model in MD, the so-called force field, crucially influences the accuracy of these simulations. Starting with the work of Perkins et al.[16,17] much effort has been made in developing force fields specifically for deep eutectic mixtures.[16–21] One adjustment, that many DES force fields have in common, is a modification of the electrostatics within the DESs.[22] Based on the force field developments for ILs,[23–26] it was found that the intermolecular attractions within ILs and DESs are systematically overestimated by force fields that use net charges of ±1 for charged molecules. *Ab initio* molecular dynamics revealed a charge transfer between the components of ILs and DESs in liquid solution.[24,27] In the developments of many non-polarizable force fields for DESs, this charge transfer is implicitly accounted for by scaling the partial charges of the DESs constituents.[16–21] However, a universal degree of charge scaling, that is applied to either only the HBA or both DES constituents, could not be found.[22] For instance for the DESs consisting of choline chloride and glycerol, Perkins et al.[16] found an optimized scaling factor of 0.9 for the charges within the HBA, whereas Doherty and Acevedo[18] and Mainberger et al.[19] achieved the best results using a factor of 0.8 and 0.75, respectively, while also scaling the charges of the HBD. Contrary to this charge scaling approach, Chaumont et al.[28] could improve the performance of the GAFF model by adjusting the Lennard-Jones (LJ) interactions rather than the partial charges of ChCl-Gly and ChCl-EG. In other cases[29–32] a non-scaled force field has been used to gain

deep insights into the structural role of water in DES/water mixtures. Although these non-polarizable force fields have proven to correctly reflect static properties and the liquid structure of DESs, the prediction of dynamic properties, such as diffusion coefficients and viscosities, was shown to be challenging.[22] Polarizable force fields can in theory provide an alternative strategy to reflect the polarization states within the DESs in the simulations and thus largely improve the prediction of dynamic properties.[33] MD simulations using polarizable force fields, on the other hand, are more computationally demanding compared to their non-polarizable counterparts, which is of particular importance for large protein systems containing more than 250000 atoms, as investigated within this article. One major aim of investigating the enzymatic behavior in DESs is the screening of different DES components, their ratio in the eutectic mixture as well as finding the optimal water content. With these screening studies in mind, the investigations within this work are restricted to commonly used non-polarizable force fields. Nevertheless, with growing computational resources polarizable force fields can offer detailed studies of specific systems of interest.

The high viscosity of many deep eutectic mixtures has become one hurdle for industrial applications[6] as well as sufficient convergence of molecular simulations. In general, the dynamic viscosity of fluids can be determined from MD simulations by equilibrium MD (EMD) and non-equilibrium MD (NEMD) methods.[34] For solutions with a high viscosity (> 5 mPa s) and therefore a slow dynamic behavior, the use of NEMD methods is suggested due to a better convergence compared to EMD.[35,36] On the other hand, EMD methods allow to simultaneously analyze other transport properties (e.g., diffusion coefficients) from the same trajectory.[36] For a thorough review on EMD to compute transport properties from MD simulations the reader is referred to Maginn et al.[35] A popular NEMD method to determine the viscosity from MD is the periodic perturbation method.[34,37] Within this method, the acceleration amplitude $A$ of an external shear field has to be selected with care, as it can distort the equilibrium, if set too high. Although different approaches of choosing this amplitude for viscosity estimates of DES systems have been used,[18,20] a systematic investigation of its influence on simulations of DESs has not been performed. Here, we present an in-depth discussion on the chosen amplitude for the system in question.

The variety of available bio-molecular force fields for DESs demands a systematic investigation of their capability for studying enzymes in DESs with MD simulations. Therefore, interaction models from three different bio-molecular force field families (CHARMM, Amber, and OPLS) are tested to represent the deep eutectic mixtures of choline chloride with glycerol or ethylene glycol. These force fields include different approaches to treat the ionic charges in the simulations and have already been applied to study DESs in the past.[16–19,31,38–41] Whereby, the here tested force fields based on Amber and OPLS have been specifically tuned towards representing DESs in the MD simulations.[16–19]

The effect of deep eutectic and organic solvents on the catalytic behavior of enzymes has mainly been studied by MD simulations for lipases[39,42–44] with these studies recently being extended to other enzyme classes.[40,41] In a prior publication[41] we presented the first investigation of alcohol dehydrogenase from horse liver (HLADH) in the DES composed of choline chloride and glycerol by experiment and simulation. Herein, HLADH is chosen as a model enzyme to systematically elucidate the force field performances for MD simulations of alcohol dehydrogenases in DESs. In addition, we emphasize that the outcome of the force field comparison within this work may also be transferrable to other enzyme simulations. Since enzymes are not functional in water free systems, a certain amount of enzyme-bound water is always needed.[45] Therefore, we investigate all systems with a DES plus water, where the water concentration is varied from 0% to 100%. First, we elucidate the force field performance for DES/water mixtures without protein. For better validations, viscosities and thermodynamic activities were determined experimentally. Thereafter, force field influences on the HLADH structure and HLADH's solvation layer in pure DES and DES/water mixtures are compared.

## METHODS

The experimental and computational methods, that are necessary to present and discuss the results of this work, are summarized in the following paragraphs.

### Experimental measurements of water activity ($a_W$) and viscosity $\eta$

Mixtures (5 mL) of ChCl-Gly or ChCl-EG with various water contents of 0–100% were freshly prepared and mixed at 60°C for 1 hour in 25 mL sealed glass bottles. The thermodynamic water activity ($a_W$) of these mixtures were then determined at room temperature (24–25°C) using HMT337 Humidity and Temperature Transmitter (vaisala, Vantaa, Finland). Here, the $a_W$ was measured based on the ratio of the water vapor pressure in the DES/water mixtures ($p$) to the vapor pressure of pure water ($p_0$).

$$a_W = p/p_0 \quad (1)$$

The dynamic viscosity ($\eta$) of the DES/water mixtures was measured on 2 mL sample with a Brookfield Digital Rheometer (Model DV-III Ultra, Brookfield Engineering Laboratories Inc., MA, USA) equipped with a spindle CPE41, at different shear rates between 0.2 $s^{-1}$ and 500 $s^{-1}$ at room temperature (24–25°C).

### Force fields

Figure 1 shows structures of choline, glycerol, and ethylene glycol. A central atom, that is needed for the calculation of solvation layers, is highlighted for each molecule.

For simulating the DESs based on the *Chemistry at Harvard Macromolecular Mechanics* (CHARMM) force field model, the topologies and parameters for choline, chloride, glycerol and ethylene glycol were taken from the *CHARMM General Force Field* (CGenFF) version 4.1.[46,47] Thereby, the force field parameters of CGenFF[46,47] were not specifically adjusted towards the DESs, but tuned to represent a variety of components (e.g., glycerol, heptane). Nevertheless, CGenFF has already been applied for studying the effect of water on the structure of ChCl-Gly[31] as well as studying the effect of ChCl-Urea on the catalytic activity of lipase[39] and lyosozyme.[40] Note, that for CHARMM refined parameters for ethylene glycol exist,[48] which were already used to simulate ChCl-EG.[49] However, to be consistent with the ChCl-Gly, we are using the original CGenFF parameters for ethylene glycol here. For all simulations within this work, that use CGenFF as model for the DES molecules, the interactions of HLADH are calculated by the CHARMM36m force field[50] with a cut-off radius $r_{cut} = 1.2$ nm for the LJ- and electrostatic interactions. The forces for the LJ-interactions are thereby smoothly switched between 1.0 and 1.2 nm.

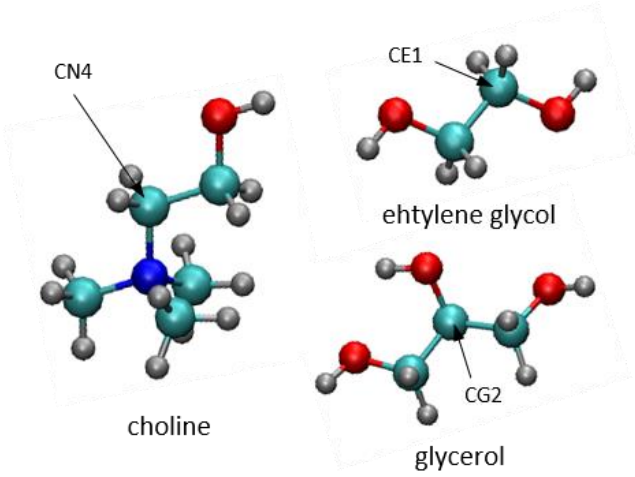


**Figure 1.** Representations of choline, glycerol and ethylene glycol as CPK model (carbon: cyan, oxygen: red, nitrogen: blue, hydrogen: grey). Central heavy atoms, that are necessary to determine the solvation layer of these molecules are highlighted. The software VMD[51,52] was used for this visualization.

The force field parameters for the simulations using the *General Amber Force Field* (GAFF) are based on the work of Perkins et al.[16,17] further referred to as GAFF-DES. They have taken the partial charges of choline chloride from a restrained electrostatic surface potential (RESP) calculation and were scaled by a factor of 0.9 in order to intrinsically represent charge transfer within the DES.[16] Lennard-Jones parameters as well as all parameters for the bonded and intra-molecular interactions were kept from the original GAFF.[53] Baz et al.[38] and Zhang et al.[54] have successfully applied this force field to study properties of ChCl-Gly and ChCl-EG, here we use the same parameters as these authors. In the simulations using GAFF-DES to represent the DES molecules, the protein interactions are modeled with the Amber03* force field.[55] Contrary to prior applications of GAFF-DES to validate the force field[16,17,19] and study the effect of water on the ChCl-Gly,[38] the simulations performed within this work use a cut-off radius $r_{\mathrm{cut}} = 0.9$ nm in accordance to the parametrization of the protein force field Amber03*.[55] In line with Amber03*,[55] the LJ-potential is thereby shifted to zero at the cut-off and analytical dispersion corrections for pressure and energy are included.

The topologies for the DES molecules based on the *Optimized Potential for Liquid Simulations – All Atom* (OPLS-AA) force field were taken from Doherty and Acevedo[18,56] and further referred to as OPLS-DES. The parameters for choline chloride were derived from prior developments of ionic liquid force fields,[57,58] whereas the parameters for the HBD (e.g., glycerol) are based on the OPLS-AA force field.[59] In contrast to the developments of GAFF-DES,[16] a charge scaling factor of 0.8 has been applied not only to choline chloride but also to the HBD. Non-bonded interactions were fine-tuned by Doherty and Acevedo[18] to fit radial distribution functions derived from ab initio MD simulations and neutron diffraction data. To represent HLADH in the simulations using OPLS-DES[18] within this work the interactions of the protein were modeled with the OPLS-AA/M force field.[60,61] Contrary to the work of Doherty and Acevedo,[18] a cut-off radius $r_{\mathrm{cut}} = 1.1$ nm was applied in accordance with the protein interaction model OPLS-AA/M.[60] The forces from the LJ-interactions were thereby smoothly switched to zero between 0.9 and 1.1 nm. Very recently the authors of the OPLS-DES force field have parametrized further DES components, whereby a different parameterization strategy was used.[62]

The TIP3P force field[63] was used to represent water in all MD simulations that are performed within this work. In case of simulations using CGenFF/CHARMM36m the CHARMM-TIP3P variant[64,65] has been used, which is a slight modification of the original TIP3P model.[63]

**Molecular dynamics simulations**

The following paragraph explains the set-up for the molecular dynamics simulations for ChCl-EG using GAFF-DES,[16] CGenFF[46,47] and OPLS-DES[18] as well as for ChCl-Gly using GAFF-DES[16] and CGenFF.[46,47] These simulations are performed with the software package GROMACS version 2019.4.[66–68] Details of the MD simulation procedure for mixtures of ChCl-Gly and water using the OPLS-DES force field[18] can be found in a prior publication.[41] For estimating time depended errors for various properties from the MD simulations the block averaging technique[69] was utilized. Details of the chosen time frames and block sizes can be found in the corresponding figure captions.

**DES/water mixtures**

The equilibration of highly viscous DES systems has been shown to be challenging.[22] To overcome the issues due to the slow dynamic behavior of many DESs, different equilibration schemes have been proposed. Based on the equilibration of polymer systems,[70] Perkins et al.[17] proposed a pressure compression and decompression scheme that consists of sub-simulations in the isothermal-isobaric (NPT) and canonical (NVT) ensemble at different temperatures and pressures. Others (e.g., Liu et al.,[71] Huang et al.[41]) have enhanced the mixing of DESs or ionic liquids by increasing and decreasing the temperature during the equilibration. Within our study we tested both approaches and found the temperature annealing similar to Liu et al.[71] to 500 K to deliver the best results based on diminishing energy drifts. Therefore, the following scheme is used to equilibrate the DES-water mixtures.

First, cubic boxes with periodic boundary conditions were built using packmol.[72] A summary of the compositions of the DES-water mixtures can be found in Tables S1 and S2 (in the SI). An energy minimization using the steepest decent algorithm for 5000 steps was followed by a 1 ns NVT simulation at 298.15 K. To integrate Newton's laws of motion the leap frog integrator[73] with a time step of 1 fs was used. The temperature of the system was adjusted by the velocity rescale thermostat[74] with a time constant of $\tau_T = 1$ ps. All bonds with hydrogen atoms were by LINCS[75] or in case of water by the SETTLE algorithm.[76] To enhance the mixing of the DES components the system temperature was increased to 500 K during 1 ns and kept at 500 K for a duration of 20 ns. In this and the following steps a time step of 2 fs was applied. The system was subsequently cooled down to 298 K during 1 ns, which was followed by a 2 ns NPT simulation. Whereby, the Berendsen barostat[77] was used to control the pressure of the system at 1 bar. Afterwards, production runs at 298.15 K and 1 bar were performed for 50 ns. The pressure control was switched to the Parrinello-Rahman barostat[78] with a time constant $\tau_P = 5$ ps and an isothermal compressibility $\kappa_T = 5 \times 10^{-5}$ bar$^{-1}$. Long-range electrostatic interactions were modeled by the smooth Particle-Mesh

Ewald[79] (PME) method with a PME order of 4 in all MD simulations. The last 20 ns of the trajectory were used to analyze hydrogen bonds, radial distribution functions (RDFs), the density $\rho$ of the solution and mean-squared displacements. Whereby, a cut-off distance donor acceptor of $r_{\mathrm{HB}} = 0.35$ nm and a cut-off angle between hydrogen – donor acceptor of $\phi_{\mathrm{HB}} = 30$ deg was used to characterize the hydrogen bonds.

**Protein simulations**

Starting with the crystallographic structure of HLADH (PDB entry 6O91),[80] cubic boxes with a box length of 13.6 nm were built and solvated using packmol.[72] Whereby, initial position of 251 water molecules, that were found to be structural relevant, were preserved. The selection of these structural water molecules was based on the experimental B-factors. With restrained positions of all heavy protein atoms, an energy minimization using the steepest decent algorithm was performed for 5000 steps. Bonds including hydrogen atoms were fixed by using LINCS[75] or in case of water using SETTLE.[76] In all MD simulations the leap frog algorithm[73] for integration the equations of motion was used. Following the energy minimization, the systems were equilibrated in five MD steps as already described in a previous publication[41] (see Figure S10 of this reference). First, a 2 ns NVT simulation at 298.15 K using a time step of 1 fs was performed. Similar to the DES-water mixtures, the temperature has afterwards been increased to 500 K during 1 ns and kept at 500 K for 20 ns by switching the time step to 2 fs. After decreasing the temperature back to 298.15 K during 1 ns, the protein structure was stepwise released in two consecutive NVT simulations for 0.5 ns by restraining the positions of the protein backbone and $C_\alpha$-atoms of HLADH, respectively. The temperature elevation combined with restraining the heavy protein atoms, protein backbone and $C_\alpha$-atoms of HLADH in the three release steps allows to improve the mixing of the solvent without distorting the protein structure. The release of the enzyme structure is followed by a 2 ns NPT equilibration at 1 bar with the Berendsen barostat.[77] Afterwards, a production run of 100 ns at 298.15 K and 1 bar (now Parrinello-Rahman barostat[78]) is performed, whereby the last 40 ns of the trajectory were used for the analysis of the protein structure and protein-solvent interactions. The same settings as for the DES-water mixtures were used to control the temperature and pressure of the system as well as model the LJ-interactions and electrostatics. To increase statistical significance, two replica simulations starting from two independent initial positions and initial velocities were performed for each data point. A summary of all compositions in the protein simulations can be found in Tables S3 and S4 (see the SI).

**Analytical methods**

Based on the NPT sampling for the DES-water mixtures further MD simulations were performed to determine the free-energy of solvation of water $G_{\mathrm{W}}^{\mathrm{solv}}$ and the dynamic viscosity $\eta$ of the solution.

Due to the ionic nature of choline chloride, the mole fraction of a component in the DES-water mixtures can be defined in different ways. Within this work the mole fraction is defined from the number of molecules in the simulation $N$ by

$$x_i = \frac{N_i}{N_{\mathrm{H_2O}} + N_{\mathrm{Ch^+}} + N_{\mathrm{Cl^-}} + N_{\mathrm{HBD}}} \tag{2}$$

treating the choline and chloride ions each as individual species.

**Determination of the free energy of solvation**

The solvation free energy $\Delta G_{\mathrm{W}}^{\mathrm{solv}}$ of water can be calculated from MD simulations by stepwise decoupling the interactions of one water molecule from its surrounding. For a smooth transition between the two states (liquid mixture and ideal gas) a scaling factor scheme has to be chosen in order to get overlapping states.[81] First the coulomb interactions of the water molecule were stepwise decoupled form its surrounding using the following linear $\lambda$-scheme: $\lambda_{\mathrm{Coulomb}}$ = (0, 0.125, 0.25, 0.375, 0.5, 0.625, 0.75, 0.875, 1). Afterwards the LJ-interactions of the decoupled water molecules were stepwise scaled by the following scheme: $\lambda_{\mathrm{LJ}}$ = (0.05, 0.1, 0.2, 0.3, 0.4, 0.5, 0.6, 0.65, 0.7, 0.75, 0.775, 0.8, 0.825, 0.85, 0.9, 0.95, 1). Whereas the LJ-potentials were modified with a soft-core potential using $\alpha_{\mathrm{SC}} = 0.5$, $\sigma_{\mathrm{SC}} = 0.3$ and a power of 1. Bonded interactions within the decoupled water molecule were preserved, which means, that the water molecule is in its ideal gas state after decoupling from the liquid solution. In case of bond constraints, a few changes had to be made compared to the NPT simulations. The LINCS[75] algorithm was used for constraining the hydrogen bonds within the decoupled TIP3P water molecule. The Fourier dihedrals[60] within the DES molecules as used in OPLS-DES[18] needed to be converted to Ryckaert-Bellemens functions. Each step in the $\lambda$-scheme was simulated for a total simulation time of 12 ns using the first 1 ns for equilibration. Whereby the last snapshot of the NPT simulations was used to start the first $\lambda$-point, the other $\lambda$-points were started from the previous steps after the simulation had reached 1 ns.

The solvation free energy for water in the respecting liquid mixture $\Delta G_{\mathrm{W}}^{\mathrm{solv}}(x_{\mathrm{W}})$ is then estimated using thermodynamic integration (TI).[82,83] Integrated curves[81] for the calculation of the solvation free energy are exemplarily shown in Figure S1 in the SI for the system of ChCl-Gly with 40 mol% water for all three investigated force fields. The activity coefficient of water in the corresponding solutions can be calculated from the difference of the solvation free energy in the DESs mixture $\Delta G_{\mathrm{W}}^{\mathrm{solv}}(x_{\mathrm{W}})$ and pure water $\Delta G_{\mathrm{W}}^{\mathrm{solv}}(x_{\mathrm{W}} = 1)$ as reference state by

$$\gamma_{\mathrm{W}} = \exp\left(\frac{\Delta G_{\mathrm{W}}^{\mathrm{solv}}(x_{\mathrm{W}}) - \Delta G_{\mathrm{W}}^{\mathrm{solv}}(x_{\mathrm{W}}=1)}{RT}\right)\frac{\rho(x_{\mathrm{W}})}{\rho(x_{\mathrm{W}}=1)} \tag{3}$$

with $\rho(x_{\mathrm{W}})$ as number density of the simulation, $R$ as universal gas constant and $T$ as system temperature.[38,84] Whereby, the number density $\rho(x_{\mathrm{W}})$ is defined by

$$\rho(x_{\mathrm{W}}) = \frac{\sum_i N_i}{\langle V(x_{\mathrm{W}})\rangle} \tag{4}$$

with $\langle V(x_{\mathrm{W}})\rangle$ as time averaged volume of the simulation before the decoupling of one water molecule. This allows the calculation of the activity of water $a_{\mathrm{W}}$ using the mole fraction $x_{\mathrm{W}}$ as defined in equation 2.

$$a_{\mathrm{W}} = \gamma_{\mathrm{W}} \cdot x_{\mathrm{W}} \tag{5}$$

In order to enhance statistical significance, replica simulations for in a minimum of three individually decoupled water molecules were performed. This means, that information from at least 1.7 µs simulation time is included in each data point.

**Determination of the dynamic viscosity**

For systems with viscosities higher than 5 mPa s, it is recommended to use a NEMD method.[35] Therefore, in this work the shear viscosity is determined by the periodic perturbation method.[34,37] In this method an external force in form of an cosine shaped shear field

$$a_x(z) = \mathcal{A}\cos\left(\frac{2\pi}{l_z}\cdot z\right) \quad (6)$$

is applied on the system with $l_z$ as length of the simulation box along the z-axis and $\mathcal{A}$ as amplitude of this acceleration field. This will result in a velocity field

$$u_x(z) = \mathcal{V}\left(1 - e^{-\frac{t}{\tau_r}}\right)\cos\left(\frac{2\pi}{l_z}\cdot z\right) \quad (7)$$

within the liquid solution, with $\tau_r$ as relaxation time of the system and $\mathcal{V}$ as amplitude of the velocity field. This velocity field can be measured and related to the viscosity using the following formula:

$$\eta = \frac{\mathcal{A}}{\mathcal{V}}\frac{\rho l_z^2}{4\pi^2} \quad (8)$$

with $\rho$ as density of the simulation box.[34] The acceleration amplitude $\mathcal{A}$ has to be chosen for the periodic perturbation method. Whereby, $\mathcal{A}$ should not be too large, as it could distort the equilibrium of the solution.[34] But it should also be large enough to get reliable statistics[34] and to be distinguishable from the thermal velocity,[85] this allows the signal-to-noise ratio to be large enough.[86] Unfortunately, there is no method how to choose the value for $\mathcal{A}$ for a specific system. Zhao et al.[87] plotted $\mathcal{A}$ against the obtained viscosity and extrapolated a linear fit to $\mathcal{A} = 0$ to obtain the viscosity for the undisturbed system. However, they noted that the assumption of a linear dependency requires further investigations.[87] Nevertheless, others have adopted this method (e.g., Doherty and Acevedo,[18] Sneha et al.[88]). For viscosity estimates of DES systems, different approaches of choosing the acceleration amplitude have been used. For example, Doherty and Acevedo[18] extrapolated the results from different amplitudes to the undistorted system. Ferreira et al.,[20] on the other side, used a fixed amplitude of $\mathcal{A} = 0.001$ nm ps$^{-2}$ for all viscosity calculations. In consequence, we investigated the influence of the amplitude over a range of three orders of magnitude on the viscosity for water, three ChCl-Gly systems, and two ChCl-EG systems (all simulated with the GAFF-DES force field) covering a wide range of viscosity magnitudes (see Figure S2 in the SI). The shape of all curves is similar, where at larger amplitudes the viscosity diverges because it decreases with increasing $\mathcal{A}$. However, for smaller $\mathcal{A}$ the viscosity converges to a fixed value. If $\mathcal{A}$ is further decreased below 0.002 nm ps$^{-2}$, the results start to fluctuate. These fluctuations and the larger error bars at lower amplitudes indicate poor statistics for these simulations. For a better comparison, these data points are normalized by the viscosity at $\mathcal{A} = 0.002$ nm ps$^{-2}$. Figure 2 summarizes the dependency of the normalized viscosity for the tested DESs systems and water. All systems show a similar trend and converge at $\mathcal{A} = 0.002$ nm ps$^{-2}$, whereas the converged region of water is larger than for the DES systems. The converged region specifies the range of amplitudes were a compromise between good statistics of the simulation without distorting its equilibrium is found. Therefore, $\mathcal{A} = 0.002$ nm ps$^{-2}$ is used for the viscosity calculations within this work.

It would be interesting to see, if such a dependency could also be found for other systems allowing to identify at which amplitudes the values converge. Ferreira et al.[20] used a fixed amplitude of $\mathcal{A} = 0.001$ nm ps$^{-2}$ to investigate DES systems, which fits to the converged region observed within this work. Zhao et al.[87] used amplitudes between 0.08 and 0.16 nm ps$^{-2}$ and found a linear relation with the viscosity for all 15 investigated systems. For this $\mathcal{A}$ range, all systems (even water) investigated here are in the region where $\eta$ is depending on $\mathcal{A}$. Importantly, the region of constant water viscosities (see Figure S2d in the SI) coincides with the TIP3P viscosity obtained earlier with the periodic perturbation method[86] ($\mathcal{A} = 0.005$ nm ps$^{-2}$) and the Green-Kubo relation.[89] Song and Dai[86] have investigated the influence of the acceleration amplitude $\mathcal{A}$ on viscosity calculations of water models (TIP5P and SPC/E) and found a stable plateau for $\mathcal{A} < 0.005$ nm ps$^{-2}$. For larger amplitudes they revealed a viscosity variation, which is in good agreement with the TIP3P dependency found in this work. A similar amplitude dependency was also shown for a different water model and methanol accompanied with a demonstration that smaller amplitudes result in larger error bars.[90]

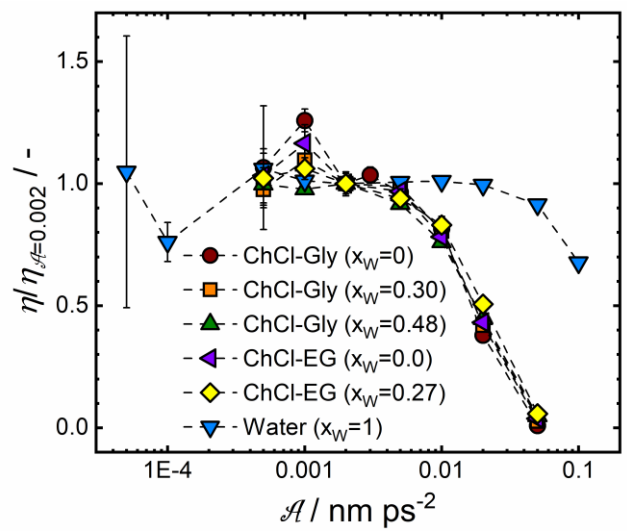


**Figure 2.** Normalized dynamic viscosity $\eta/\eta_{\mathcal{A}=0.002}$ of mixtures of ChCl-Gly or ChCl-EG and water from molecular dynamics simulations using GAFF-DES[16] and TIP3P[63] in dependency of the amplitude $\mathcal{A}$. The viscosity is determined by the periodic perturbation method and normalized by the viscosity of the simulation using the amplitude $\mathcal{A} = 0.002$ nm ps$^{-2}$ for comparison. The dashed lines are added to guide the eye.

A theoretical error estimation can be used to optimize the simulation set-up.[34] The error $\sigma_\eta$ is calculated from the geometry of the simulation box and the sampling time $t_a$ by

$$\sigma_\eta = \frac{4\pi\eta^{\frac{3}{2}}}{\mathcal{A}\rho l_z}\sqrt{\frac{k_B T}{t_a V}} \quad (9)$$

with $k_B$ as Boltzmann constant, $T$ as system temperature and $V$ as volume of the simulation box.[34] From equation 9 it can be seen that the shape of the simulations box can be altered to improve the accuracy of $\eta$. Therefore, cuboid simulation boxes that are elongated along the z-axis ($l_z = 20$ nm) were built using packmol[72] with densities from the prior NPT simulations. The number of DES and water molecules was increased by a factor of 1.5 for better statistical behavior (Table S5 in the SI). After an energy minimization, the NVT simulations, that are used for the viscosity estimates, were equilibrated using the same temperature annealing scheme as the NPT simulations. However, the 2 ns NPT equilibration is not necessary for the NVT simulations and has therefore been omitted. After the equilibration, the acceleration field with an amplitude of $\mathcal{A} = 0.002$ nm ps$^{-2}$ was applied and a sampling of the velocity field was performed for a simulation time of 105 ns with the last 100 ns for sampling. In the case of large viscosities (> 150 mPa s) the simulation time was increased to 305 ns for a

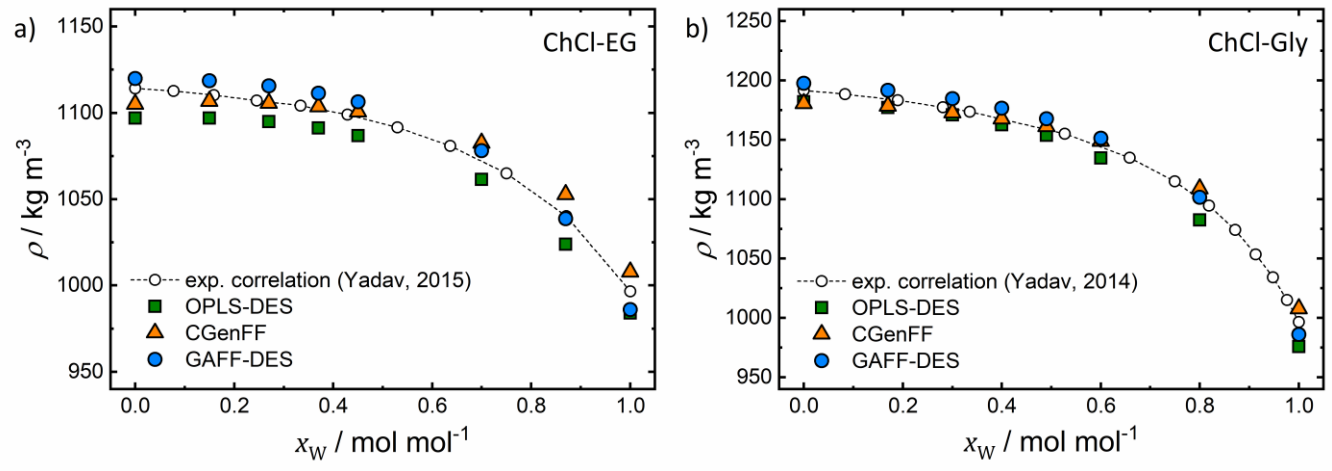


**Figure 3.** Time averages of the density $\rho$ at 298 K and 1 bar of ChCl-EG (a) and ChCl-Gly (b) in mixtures with water as function of the water mole fraction $x_W$ from molecular dynamic simulations over the last 20 ns of the trajectory in comparison to the experimental correlations from Yadav et al.[91,92] The error estimates are 95% confidence intervals from block averages over the last 20 ns of the trajectory with a block size of 2 ns and smaller than the symbol size. Blue circles: GAFF-DES,[16] green squares: OPLS-DES[18] and orange triangles: CGenFF.[46,47] The dashed line is added to guide the eye.

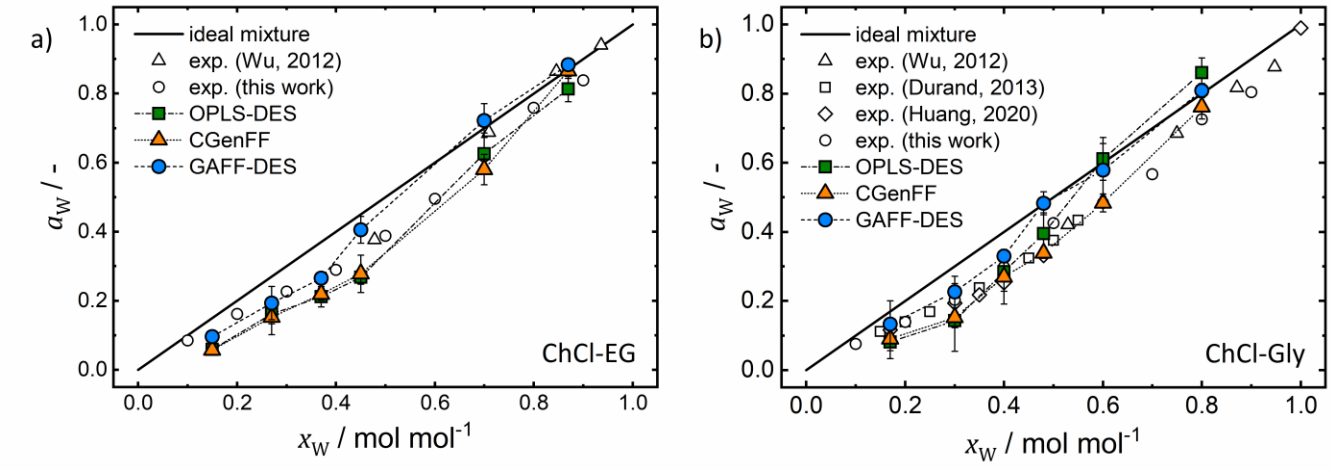


**Figure 4.** Thermodynamic activity $a_W$ of water at 298.15 K and 1 bar in aqueous mixtures of ChCl-EG (a) and ChCl-Gly (b) in dependency of the water mole fraction $x_W$ estimated from molecular dynamic simulations in comparison to literature experimental values (open triangles: Wu et al.,[93] open squares: Durand et al.,[94] open : Huang et al.[41]) and experimental data measured within this work (open circles). The activity of water $a_W$ is calculated from the Gibbs-Free energy of solvation for water using Eqs. 2-4. The error bars correspond to the standard deviation of in minimum three replica simulations of three individually decoupled water molecules. Blue circles: GAFF-DES,[16] green squares: OPLS-DES[18] and orange triangles: CGenFF.[46,47] The dashed and dotted lines are added to guide the eye.

better convergence. For this simulation set-up, the errors calculated from the trajectories (block averaging) of the systems, that were used to test the amplitudes, coincide well with the theoretical error from equation 9. (Figure S3 in the SI). Only for large amplitudes, which resulted in smaller viscosities, the simulated errors are higher than the theoretical ones.

## RESULTS AND DISCUSSION

In the following paragraphs the three force fields GAFF-DES,[16,17] CGenFF[46,47] and OPLS-DES[18] are systematically tested and validated for simulating ChCl-Gly and ChCl-EG in mixtures with water. The goal of this comparison is to elucidate the strengths and weaknesses of each model.

### Validation of force fields for deep eutectic solvents

The performance of MD simulations strongly depends on the used interaction model. Before combining the DESs with an enzyme, the DES model performance should be validated without the presence of a macromolecule. For this purpose, the liquid density $\rho$, the thermodynamic activity of water $a_W$ and the dynamic viscosity $\eta$ are determined from MD simulations and compared to experimental measurements and literature data. Besides the calculation of bulk phase properties, a key strength of MD simulations is the in-depth understanding of the microstructure of DESs. Therefore, the important interactions within the DES/water mixtures are assessed by determining characteristic radial distribution functions and hydrogen bond interactions.

**Static properties of deep eutectic solvents**

Although the liquid density $\rho$ is rarely used for directly fitting force field parameters, it often delivers a good initial impression of the accuracy of the interaction models. The simulated room temperature densities $\rho$ of mixtures of ChCl-EG and ChCl-Gly with water are shown in Figure 3. In general, all three tested force fields describe the density in quantitative agreement (max. 2% deviation) with the experimental correlation from Yadav et al.[91,92] This accurate prediction of the liquid density for scaled and non-scaled non-polarizable force fields is consistent with the reported densities of recent developments of DESs interaction models.[22]

The thermodynamic activity of water $a_W$ is an important property to understand enzyme hydration in non-aqueous reaction media. For instance, Wedberg et al.[43] linked the bulk phase water activity to the hydration of *Candida antarctica* lipase B (CALB) in different organic solvents. In order to study this effect for enzymes in solutions with a low water content, the force fields have to correctly reflect the activity of water in these mixtures.

Figure 4 shows the activity of water $a_W$ at room temperature in mixtures of ChCl-Gly and ChCl-EG with water determined from MD simulations in comparison to experimental measurements performed within this work and literature values.[41,93,94] The experiments (open symbols) show a negative deviation from the ideal behavior (solid line) for both DES/water mixtures, which indicates attractive interactions between water and the DES components. CGenFF and OPLS-DES show similar results for the activity of water in ChCl-EG. They underestimate the activity at low water concentrations ($x_W < 0.5$) but have a good agreement with the experiments for a large water content. GAFF-DES, on the other side, shows a better agreement with the experiments for low water concentrations ($x_W < 0.4$), however, for larger concentrations it rather predicts an ideal behavior than the measured negative deviation. In case of ChCl-Gly, CGenFF shows a similar behavior to ChCl-EG by slightly underestimating the activity for low water concentrations and giving a good description of $a_W$ at larger water contents. Despite using up to five replica simulations, this underestimation at 30 mol% and 17 mol% water may be the result of a bad statistical behavior of these simulations as indicated by large error estimates. While OPLS-DES gives comparable activities for low water contents, it predicts a positive deviation for 80 mol% of water, which disagrees with the experiments. GAFF-DES gives a similar curve for the activity as in ChCl-EG. The simulations show a good agreement for low water concentrations (< 40%) but predict an ideal behavior for large $x_W$. This contradicts the findings of Baz et al.[38] as they observed a good agreement with experimental measured $a_W$ in ChCl-Gly throughout the entire water concentration range using the same GAFF-DES with a different cut-off $r_{cut} = 1.5$ nm for the LJ- and electrostatic interactions. Though, Baz et al.[38] performed the MD simulation at elevated temperatures of 320.15 K and 360.15 K instead of 298.15 K as within this work. It has to be noted, that the choice of the cut-off radius may have an impact on the solvation free energy of water in solutions with a high ion density. Free-energy estimates from simulations using a larger cut-off of $r_{cut} = 1.5$ nm for GAFF-DES resulted in a slightly lower value of $\Delta G_W^{solv} = -23.627 \pm 0.379$ compared to $\Delta G_W^{solv} = -23.582 \pm 0.157$ for $r_{cut} = 0.9$ nm. However, this difference is not significant due to the large uncertainties obtained in the free-energy calculation. Concerning the activity calculations from MD simulations in general, there are two opposing effects influencing its accuracy. As already pointed out by Baz et al.[38] the calculations of the activity imply a large sensitivity towards the solvation free energy estimates. This effect becomes in particular pronounced for large water concentrations. The sampling quality, on the other hand, is much better at larger water contents and reduced at high DES concentrations due to a slow dynamic behavior.

To the best of our knowledge this work includes the first presentation of thermodynamic activity data calculated for ChCl-Gly and ChCl-EG using CGenFF and OPLS-DES, whereas Baz et al.[38] already published a study of the thermodynamic activity of water in ChCl-Gly using GAFF-DES. Overall, the non-scaled CGenFF[46,47] force field gives a good description of the thermodynamic activity of water in the investigated DES/water mixtures in particular for large water contents. This agrees with prior force field developments, which showed that static properties of DESs can be well reproduced in MD simulations by non-scaled interaction models.[22] While OPLS-DES[18] can be used in a similar fashion for ChCl-EG, it predicts a positive deviation in ChCl-Gly for large water concentrations making it less applicable to these ChCl-Gly/water mixtures. In the case of water contents below 40 mol% water, GAFF-DES,[16,17] which uses scaled electrostatics, delivers better results than CGenFF[46,47] but fails to predict the negative deviation at large water contents for both tested DESs.

**Dynamic viscosity**

Correctly reflecting the dynamic behavior of DESs in MD simulations has been a large hurdle for the developments of non-polarizable DESs force fields. For Interaction models that are not fine-tuned towards DESs, an overestimation of the electrostatic interactions between the DES molecules usually resulted in a poor description of dynamic properties such as underestimated self-diffusion coefficients and overestimated viscosities.[22] To implicitly include polarization effects within the DES, a reduction of the electrostatic interactions, e.g., by scaling the partial charges of the DES molecules, has often improved the predictions of dynamic properties by the DESs force fields.[22] In contrast to this widely used approach, Chaumont et al.[28] accomplished a similar improvement in the description of self-diffusion coefficients for ChCl-Gly and ChCl-EG by adjusting the Lennard-Jones parameters of the oxygen and hydrogen of the hydroxyl groups for GAFF.

As representative for the dynamic behavior within the MD simulations the three investigated force fields are tested to reproduce the dynamic viscosity $\eta$ of DES/water mixtures. The viscosity is a collective variable, which includes contributions from every molecule within the solution, and is much easier to access in an experiment compared to for example, self-diffusion coefficients. Figure 5 displays viscosity estimates from the periodic perturbation method[34,37] at 298.15 K and 1 bar in comparison to experimental measurements for varying water contents. The viscosity measurements of this work are in line with recently reported experimental studies for ChCl-EG and ChCl-Gly in mixtures with water.[91,95] The experiments show an exponential decrease from 325 mPa s and 41 mPa s for ChCl-Gly and ChCl-EG, respectively, down to the viscosity of pure water. In case of ChCl-Gly inconsistencies in the viscosity measurements have been reported in the literature. While the experimental viscosities of ChCl-Gly with $x_W = 0$ given in Figure 5 range between 325 mPa s and 365 mPa s, a different value of 259 mPa s was found by Abbot et al.[96] Yadav et al.[91] explained

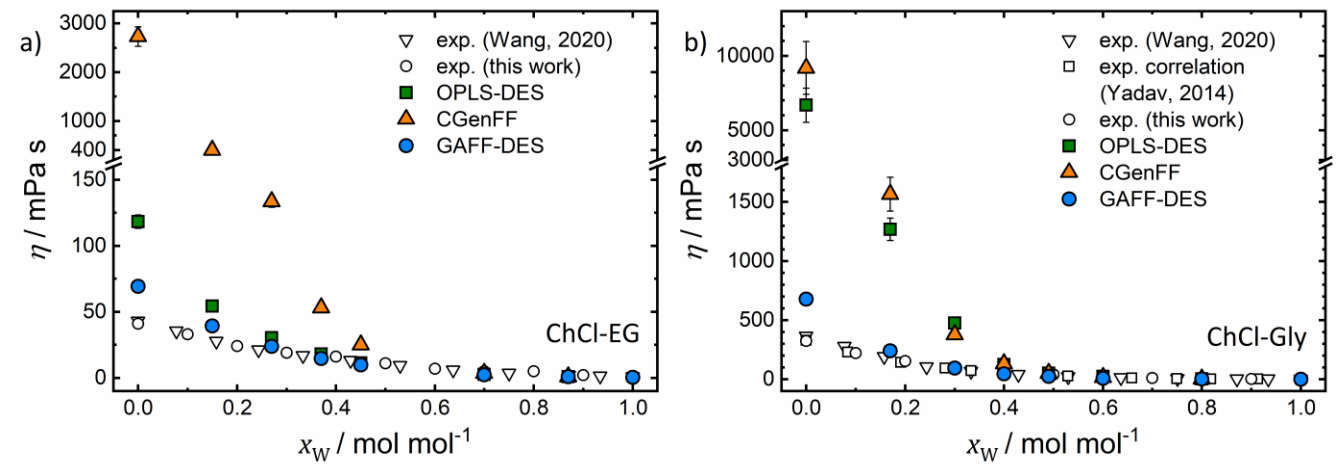


**Figure 5.** Time averages of the dynamic viscosity $\eta$ of ChCl-EG (a) and ChCl-Gly (b) in mixtures with water at 298 K and 1 bar in dependency of the water mole fraction $x_W$ from molecular dynamics simulations in comparison to experimental measurements (open circles) and literature experimental values (open squares: Yadav et al.,[91] open down-pointing triangles: Wang et al.[95]). The periodic perturbation method with an amplitude of 0.02 nm ps$^{-2}$ is used to estimate the viscosity from the NVT simulations. The error bars are 95% confidence intervals of block averages over the last 100 ns of the trajectory with a block size of 5 ns. In case of viscosities above 500 mPa s, the error bars are calculated from block averages over 300 ns with a block size of 30 ns and in case of water from block averages over 50 ns with a block size of 5 ns. Blue circles: GAFF-DES,[16] green squares: OPLS-DES[18] and orange triangles: CGenFF.[46,47]

this difference by a higher moisture in the samples of Abbott et al.[96] While the viscosity estimates from all simulations qualitatively reflect the exponential decrease, the results reveal large quantitative differences at low water concentrations between the tested force field models. The non-scaled CGenFF significantly overestimates the dynamic viscosity for both DES/water mixtures and in particular for low water contents (< 50 mol%) by up to two orders of magnitude. To probe the influence of the charge transfer, an ad hoc scaling of the electrostatic interactions for choline and chloride in CGenFF by a factor of 0.9 was tested. Indeed, the viscosity could be reduced significantly (Figure S4 in the SI). The obtained viscosities are comparable with the ones from GAFF-DES, where also a scaling of 0.9 was used. However, rigorously developing a fine-tuned DESs force field from CGenFF would demand further adjustments. Nevertheless, this demonstrates why the charge transfer was implicitly included in the non-polarizable force fields. The two scaled force fields GAFF-DES and OPLS-DES deliver a much better description of the dynamic viscosity for ChCl-EG that are in line with previous reported values. Comparing with our GAFF-DES result, Zhang et al.[54] found a similar viscosity for pure ChCl-EG (also GAFF-DES) using a Green-Kubo approach, which again testifies our choice of the amplitude $\mathcal{A} = 0.002$ nm ps$^{-2}$. Celebi et al.[97] used the Einstein relation to calculate viscosities (303 – 363 K) for ChCl-EG from simulations with the GAFF-DES force field. Comparing their results with the experimental data of Wang et al.,[95] shows also an overestimation of the viscosity. Despite including charge scaling factors, OPLS-DES significantly overestimates the viscosities for ChCl-Gly at low water contents. The close agreement of OPLS-DES with the experimental viscosity at 298 K as reported by Doherty and Acevedo[18] could not be reproduced within this work, although the radial distribution functions for pure ChCl-Gly (Figure 6) are in agreement with the values given in Ref 16. They have introduced the OPLS-DES force field and found $\eta = 258.8$ mPa s for ChCl-Gly and $\eta = 38.5$ mPa s for ChCl-EG while using a set of acceleration amplitudes and extrapolating to $\mathcal{A} = 0$. The chosen amplitudes of Doherty and Acevedo[18] are in the range of 0.04 to 0.24 nm ps$^{-2}$, but neither the exactly used amplitudes nor the $\mathcal{A} - \eta$ dependencies for the different DESs were specified. In the methods section we have discussed the periodic perturbation methods in detail and found, in agreement with others,[86,90] a plateau region, where $\eta$ is independent of $\mathcal{A}$. For example, the viscosity for water should be taken from the plateau region (see Figure S2d in the SI), as this corresponds with the reported literature value for TIP3P, whereby it was obtained with different methods.[86,89] Using larger amplitudes and extrapolating, would lead to different results. Therefore, the discrepancies between our results and Doherty and Acevedo[18] are likely due to their extrapolation to $\mathcal{A} = 0$. A plateau region could probably not be observed in their work because of the applied amplitude range. Jahn et al.[98] investigated different OPLS-variants and found that the CCCO, OCCO, and HOCH dihedrals of glycerol in the OPLS-AA force field have a large influence on glycerol's dynamic properties and microstructure. Tuning these three dihedrals[98,99] could significantly improve the self-diffusion coefficient of glycerol, which was underestimated by two orders of magnitude by the original OPLS-AA parametrization.[98] We adjusted these dihedrals in the OPLS-DES force field (Table S6 in the SI), which could drastically reduce the viscosity of pure ChCl-Gly to be in the same order of magnitude as GAFF-DES and an ad-hoc scaled CGenFF version (Figure S5).

GAFF-DES shows in general the best quantitative agreement with the experiments for both DES/water mixtures, though, it still overestimates the viscosity for the pure DESs by a factor of two. This is supported by the viscosity estimates provided by Baz et al.[38] as they observed an overestimation of the viscosity of ChCl-Gly and water mixtures by GAFF-DES at 298 K and 320 K. The order and differences of the viscosities for the water free systems of the different force fields are supported by the mean-squared displacements for chloride shown in Figure S6 of the SI. These mean-squared displacements were calculated from the NPT simulation trajectories (see Methods section). For the systems with viscosities > 1000 mPa s the

movement is extremely limited, which was also confirmed by visual inspection.

The findings of this work emphasize that, in accordance with the literature,[16–20,22] a scaling of electrostatic interactions is a viable tool to overcome the limitations of non-polarizable force fields for DESs and to correctly reflect their dynamic behavior. However, if a charge scaling is necessary and the only way to improve non-polarizable force fields remains to be an open discussion.[28] In general, GAFF-DES provides the best representation of the viscosity of ChCl-EG and ChCl-Gly in the MD simulations with CGenFF not being suitable to calculate the viscosity of DESs at water contents below 50 mol%. While OPLS-DES delivers a reasonable description of the viscosity of ChCl-EG, it underperforms for the dynamic behavior of ChCl-Gly.

**Interactions within the deep eutectic solvent**

Besides the determination of physiochemical properties of the DESs, MD simulations offer deep insights into their microstructure und provide a suitable tool to understand the interactions within a DES. This can help to reveal the origin of DESs as well as to design future deep eutectic mixtures. For a thorough review about the interactions within different DESs the reader is referred to the review of Wagle et al.[100] In the following, radial distribution functions of important interactions between the DES components as well as characteristic hydrogen bond interactions are discussed. A validation of these properties with experimental measurements is rather difficult, hence, the radial distribution functions and hydrogen bonds are only compared between the three force fields. Nevertheless, this comparison can identify differences in the description of the DESs characteristics by the force fields.

Figure 6 shows radial distribution functions for some representative interactions between the oxygens of the HBDs ($O_{Gly}$: all three oxygen of glycerol and $O_{EG}$: both oxygen of ethylene glycol), the chloride ion (Cl) and the oxygen from the choline ion ($O_{Ch}$). In case of the glycerol – glycerol interactions (Figure 6b) all three force fields show similar peaks although slightly shifted in their location. CGenFF, however, deviates from the other force fields for the description of the ethylene glycol – ethylene glycol RDFs (Figure 6a) by showing a much lower height for the first peak. Though GAFF-DES and CGenFF show identical peaks for the choline – chloride (Figure 6e-f) interaction, the radial distribution functions for chloride – HBD (Figure 6c-d) results in a smaller peak height for GAFF-DES. This reflects the charge scaling of choline and chloride, that has been implemented in GAFF-DES. The observed peak positions for the chloride interactions in CGenFF and GAFF-DES are in close agreement with the radial distribution functions provided by Weng and Toner[31] and Baz et al.[38] The interactions of chloride with the other components in OPLS-DES, on the other side, are not as pronounced as for the other force fields with the exception of chloride – ethylene glycol (Figure 6f). Nevertheless, the presented RDFs for OPLS-DES are in agreement with the published data from Doherty and Acevedo.[18] In general, the sharp peaks in the radial distribution functions of the chloride ion with the oxygen of the HBD and HBA (Figure 6c-f) highlight the important role of chloride that is bridging the interactions between HBA and HBD in choline chloride-based DESs.[31] This is supported by the fact that the interactions between choline – choline (Figure 6i-j), choline – HBD (Figure 6g-h) and HBD – HBD (Figure 6a-b) are much weaker compared to the other ones. For these interactions GAFF-DES and CGenFF show similar characteristics with the exception of the first peak missing in the choline – choline radial distribution functions for GAFF-DES, which has already been pointed out.[38] This hints that no hydrogen bonds are formed between two choline molecules in GAFF-DES. In case of OPLS-DES, the radial distribution functions rather show a flat plateau than distinct peaks for the choline – choline as well as the choline – HBD interactions.

In summary, the comparison of radial distribution functions shows that besides including different treatments of the charges all force fields display the DES characteristics consistently and in qualitative agreement. The largest deviation between the force fields were found for chloride, where the RDFs of CGenFF and GAFF-DES reflect the charge scaling.

Deep eutectics are known for their typically strong hydrogen bond interactions. Simulations on the molecular level can unravel these interactions and identify the role of a water on the microstructure of deep eutectic mixtures. Figure 7 and 8 display the characteristic hydrogen bonds that are present in ChCl-Gly and ChCl-EG, respectively. The values of the different force fields are normalized by the number of choline chloride molecules in the simulations for comparison purposes. In case of ChCl-Gly, the hydrogen bonds between water and the DES components are similarly increasing with varying water content for all three force fields with the exception of the glycerol – water hydrogen bonds for OPLS-DES (Figure 7e). Surprisingly, the number of hydrogen bonds between water and glycerol formed by OPLS-DES are constant instead. Combined with the increase of the glycerol – glycerol (Figure 7c) and simultaneous rapid decrease of the choline – glycerol hydrogen bonds (Figure 7b), which are not present for the other force fields, this indicates a separation of a glycerol phase with increasing water contents. Figure 9 reveals this unusual formation of glycerol self-aggregation (yellow) in the simulation using OPLS-DES for ChCl-Gly at 80 mol% water. This observation is a clear indication of phase separation. While such an arrangement of glycerol is neither observed in the experiment nor present for the other two interaction models (Figure S7 in the SI), it strongly suggests being a force field artifact within OPLS-DES. It has to be mentioned, that a testing of the TIP4P[63] force field for water and an increased cut-off radius for the LJ- and electrostatic interactions could not resolve this cluster formation. Because, in contrast to GAFF-DES, OPLS-DES also scaled the charges of glycerol,[18] a simulation using glycerol parameters that are rescaled has also been performed. The phase separation also occurred for this simulation using the modified OPLS-DES, which proves that the scaling of the HBD in OPLS-DES does not induce this behavior. In addition, the CCCO, OCCO, and HOCH dihedrals in glycerol in the OPLS-AA force field have proven to drastically affect the microstructure of glycerol.[98] However, adjusting these dihedrals accordingly[98,99] (see Table S6) could not resolve the observed phase separation. Molecular dynamics studies already revealed a heterogeneity in the DES microstructure structure,[22,101–103] however, it did not appear to such a large degree. Besides this study of OPLS-DES a similar phase separation phenomenon for ChCl-Gly/water mixtures at 90 mol% water was observed by Ahmadi et al.[30] in their MD simulations using the GROMOS force field 53A6.

GAFF-DES and CGenFF, on the other hand, describe the hydrogen bonds within the DESs in a consistent manner without predicting a phase separation. Instead, the number of hydrogen bonds formed between the DES constituents decrease, if the amount of water in the system is raised. This dependency agrees

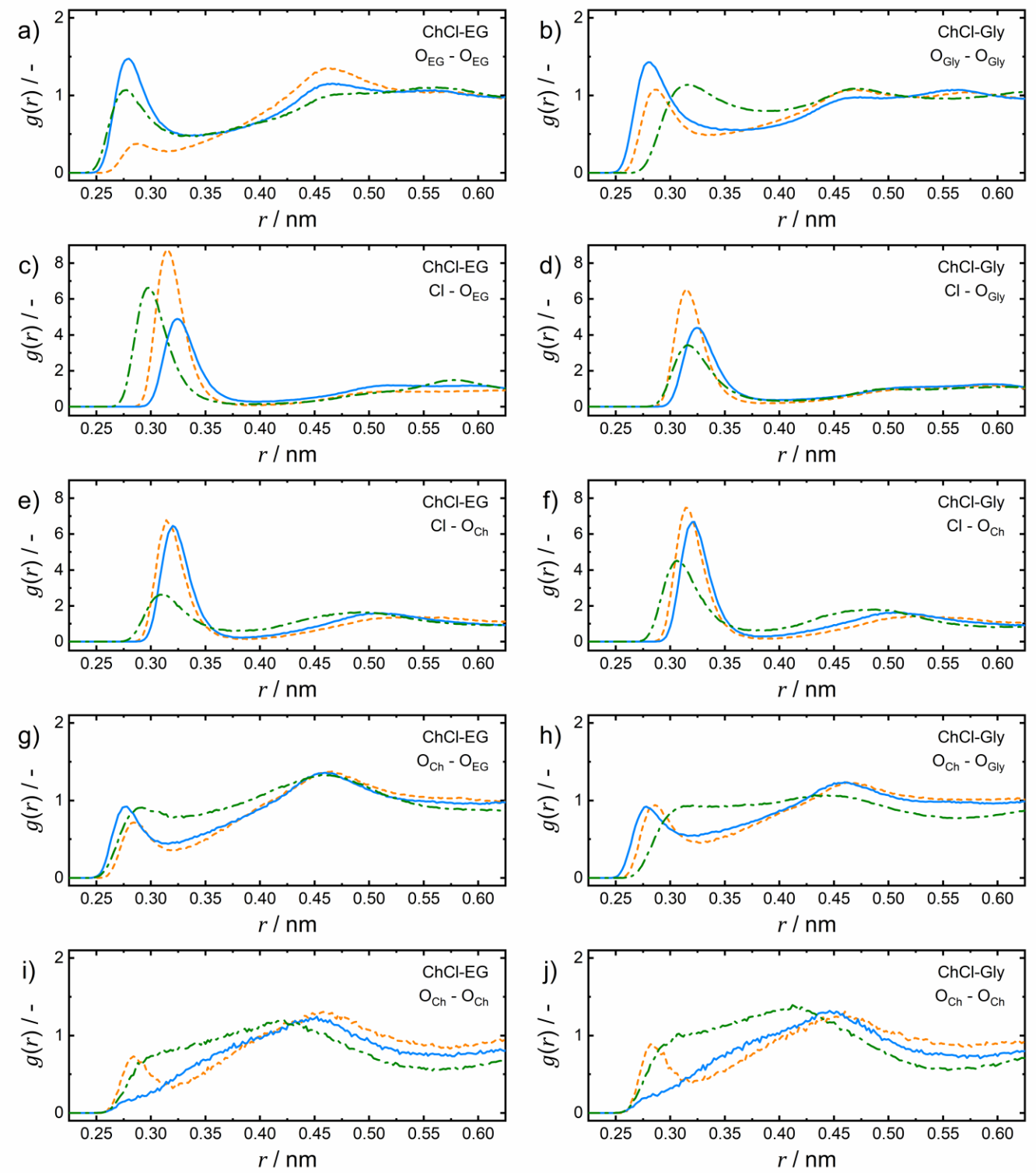


**Figure 6.** Radial distribution functions for the pure DES at 298.15 K between representative atoms within ChCl-EG (left) and ChCl-Gly (right). The representative atoms include the oxygen of choline ($O_{Ch}$), the chloride atom (Cl), both oxygen of ethylene glycol ($O_{EG}$) and all three oxygen of glycerol ($O_{Gly}$). The radial distribution functions were calculated from the last 20 ns of the trajectories. Solid blue line: GAFF-DES,[16] dash-dotted green line: OPLS-DES[18] and dashed orange line: CGenFF.[46,47]

with the data provided by Baz et al.[38] (GAFF-DES) and supports the interpretation of the effect of water on the DES structure given by Ma et al.[104] They describe the arrangement of DES/water mixtures with increasing water content in three phases. First, water diffuses into the DES super cluster and therefore its characteristics do not change considerably. By adding more water to the system, water breaks the super cluster into smaller clusters until the DES components are completely dissolved and individually hydrated.[104] In the data of CGenFF, a small difference occurs at low water concentrations, where the choline – glycerol hydrogen bonds (Figure 7b) exhibit a small increase. Weng and Toner,[31] who also observed this trend using

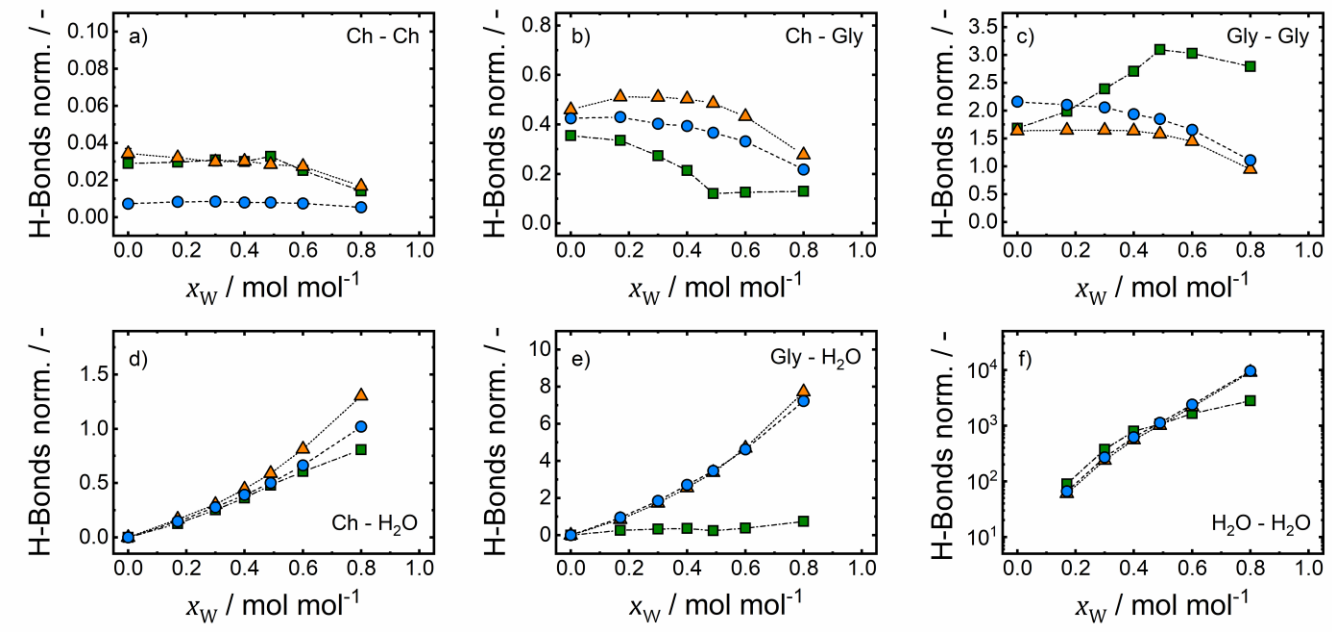


**Figure 7.** Normalized number of hydrogen bonds ($r_{HB} = 0.35$ nm, $\phi_{HB} = 30$ deg) between choline (Ch), glycerol (Gly) and water ($H_2O$) within mixtures of ChCl-Gly and water from molecular dynamics simulations in dependency of the water mole fraction $x_W$. The normalization is performed based on the number of choline chloride molecules in the simulations in the solution for comparison. The data points are time averages over the last 20 ns of the trajectories. The estimated errors are 95 % confidence intervals from block averages with a block size of 2 ns and smaller than the symbol size. Blue circles: GAFF-DES,[16] green squares: OPLS-DES[18] and orange triangles: CGenFF.[46,47] The dashed and dotted lines are added to guide the eye.

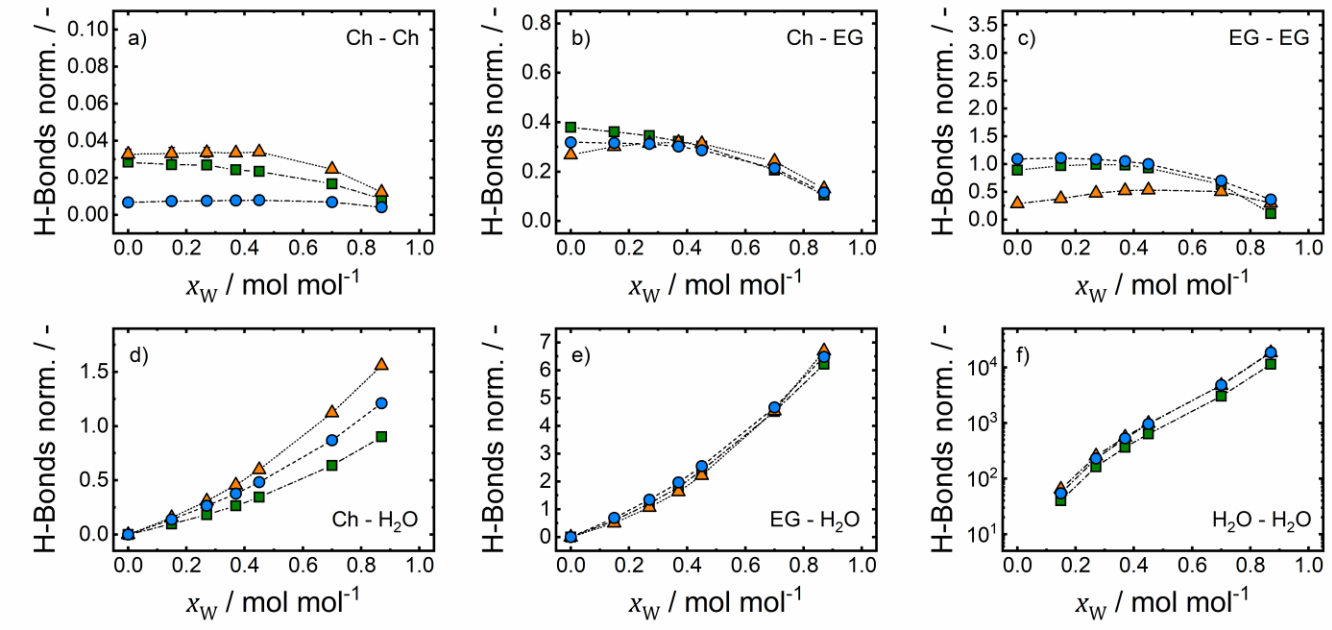


**Figure 8.** Normalized number of hydrogen bonds ($r_{HB} = 0.35$ nm, $\phi_{HB} = 30$ deg) between choline (Ch), ethylene glycol (EG) and water ($H_2O$) within mixtures of ChCl-EG and water from molecular dynamics simulations in dependency of the water mole fraction $x_W$. The normalization is performed based on the number of choline chloride molecules in the solution for comparison. The data points are time averages over the last 20 ns of the trajectories. The estimated errors are 95 % confidence intervals from block averages with a block size of 2 ns and smaller than the symbol size. Blue circles: GAFF-DES,[16] green squares: OPLS-DES[18] and orange triangles: CGenFF.[46,47] The dotted and dashed lines are added to guide the eye.

CGenFF, described water as having a "Janus-faced" role on the DES structure of ChCl-Gly. They state that at low concentrations water can intensify the DES hydrogen bond characteristics up to 35.8 wt% until water starts to break the DES structure apart. While this structure enhancing effect of water can be seen in the CGenFF data, it is not observed in the simulations of GAFF-DES. In case of GAFF-DES, the hydrogen bonds between the DES constituents instead decrease steadily over the

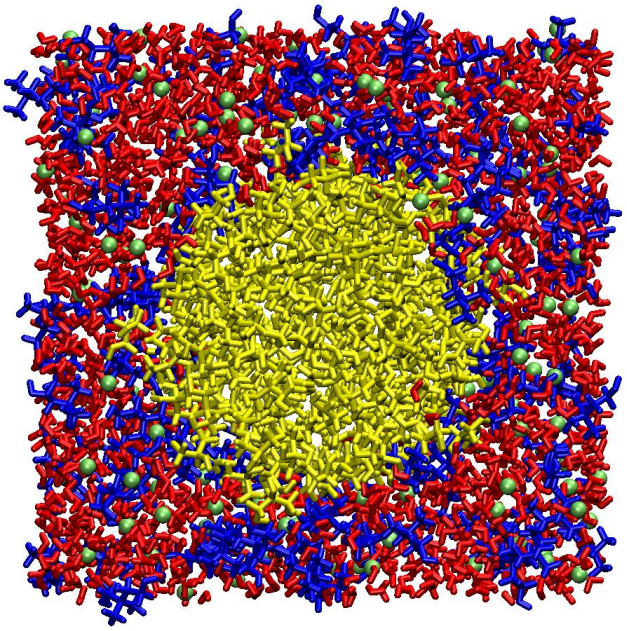

**Figure 9.** Snapshot of the molecular dynamics simulation of ChCl-Gly-water at 80 mol% water using the OPLS-DES[18] force field. Glycerol (yellow), choline (blue) and water (red) are displayed as licorice and chloride (green) is displayed as a VDW-sphere with the sphere radius scaled by a factor of 0.5. VMD[51,52] was used for visualization.

entire concentration range, suggesting that water does not have such a structure improving effect.

The hydrogen bonds of ChCl-EG (Figure 8) give a similar picture of the DES-DES and DES-water interactions compared to ChCl-Gly, that are consistent with the radial distribution function depicted in Figure 6. With increasing water content, the hydrogen bonds between water and the ChCl-EG become more probable and the characteristic interactions within the DES weaken. This diminishing effect, however, is reduced at low water concentrations indicating that water diffuses into the DES structure before breaking the interactions within ChCl-EG apart. In contrast to ChCl-Gly, no phase separation is observed for OPLS-DES. Instead, it gives a similar depiction of the DES interactions as the other force fields. Interestingly, the hydrogen bond data of ChCl-EG generated with CGenFF would lead to a similar interpretation of a structure enhancing effect of water on the DES structure at low water concentrations, as stated by Weng and Toner[31] for ChCl-Gly. However, the results of GAFF-DES and OPLS-DES do not support such a conclusion.

### The behavior of HLADH in DES/water mixtures

After the validation of the three force fields GAFF-DES,[16,17] OPLS-DES[18] and CGenFF,[46,47] these interaction models are combined with the corresponding protein parameters (Amber03*,[55] OPLS-AA/M,[60] CHARMM36m[50]). The goal of this chapter is to elucidate the differences of the force fields in order to find the best force field for investigating the behavior of HLADH in these DES/water mixtures. Such a molecular dynamics study can support the experimental investigation to gain deeper insights into the behavior of enzymes in DES-water mixtures.[39–42] Therefore, representative structural properties of HLADH and its interactions with the solvents are monitored and discussed. The phase separation observed in the MD simulations of ChCl-Gly/water mixtures using OPLS-DES clearly invalidates the usage of the force field for this case. As such a phase separation has also been observed for a different force field,[30] the simulations of HLADH in ChCl-Gly using OPLS-DES are included in order to discuss the implications of such a force field artifact on protein simulations in DESs.

Figure 10 summarizes characteristic properties that reflect the enzyme structure in various DES/water mixtures for ChCl-EG (Figure 10a-c) and ChCl-Gly (Figure 10d-f). Figure 10a+d show the root mean square deviations (RMSD) of all $C_\alpha$-atoms of HLADH in comparison to the crystallographic structure (PDB entry 6O91[80]). Figure 10b+e summarize the number of hydrogen bonds that are formed between amino acids within the enzyme and Figure 10c+f display the flexibility of all $C_\alpha$-atoms of HLADH expressed as root mean square fluctuations (RMSF). In a prior publication[41] some flexible parts of the enzyme structure were omitted in the calculations of the RMSD and RMSF due to their large impact on these properties. However, since these flexible regions may change for different force fields, all structural properties discussed within this work are calculated from all $C_\alpha$-atoms of HLADH. Figure S8 (see the SI) shows the difference between the RMSD and RMSF from this work (only OPLS-DES/OPLS-AA/M) and the data published by Huang et al.[41]

The RMSD (Figure 10a+d) of HLADH in ChCl-EG and ChCl-Gly gives a similar dependency of the water concentration for all three fore fields. In highly concentrated DES solutions, the enzyme structure is much closer to the crystallographic structure than in an aqueous environment. The data of the radius of gyration (Figure S9 in the SI) support this statement. The RMSD also indicates that the structure of HLADH in low water media differs from the structure in pure water, which might have implications on its enzymatic activity. Even the simulations with OPLS-DES representing ChCl-Gly give a similar trend compared to the other force fields. This indicates that the protein structure is not significantly affected by the observed phase separation for ChCl-Gly by OPLS-DES. The largest discrepancy in the RMSD between the three force fields occurs at 100 mol% water. While CGenFF/CHARMM36m and GAFF-DES/Amber03* give a comparable value at these concentrations, the simulations of HLADH in OPLS-DES/OPLS-AA/M result in a much lower RMSD. The difference between AMBER- and CHARMM-based force fields and OPLS and GROMOS force fields were recently also shown by Petrovic et al.,[105] where their study revealed a better performance of AMBER and CHARMM.

The decrease in intra-protein hydrogen bonds (Figure 10b+e) shows that the enzyme actively alters its surface for the interaction with water. Being smaller – as well as more mobile – than choline or glycerol and providing a good hydrogen bond interaction partner, water is able to diffuse into the enzyme structure and replace the intra-protein hydrogen bonds. Although all three force fields describe the hydrogen bonds within the protein in qualitative agreement, quantitative differences occur. OPLS-AA/M generally predicts a larger amount of intra-protein hydrogen bonds, in particular in pure water. This confirms, that HLADH arranges in a different structure in the aqueous environment in the simulations using OPLS-AA/M compared to the other two force fields. GAFF-DES/Amber03*, on the other hand, displays the lowest number of intra-protein hydrogen bonds in particular at low water contents. CGenFF/CHARMM36m shows similarities with OPLS-DES/OPLS-AA/M in the number of hydrogen bonds at water

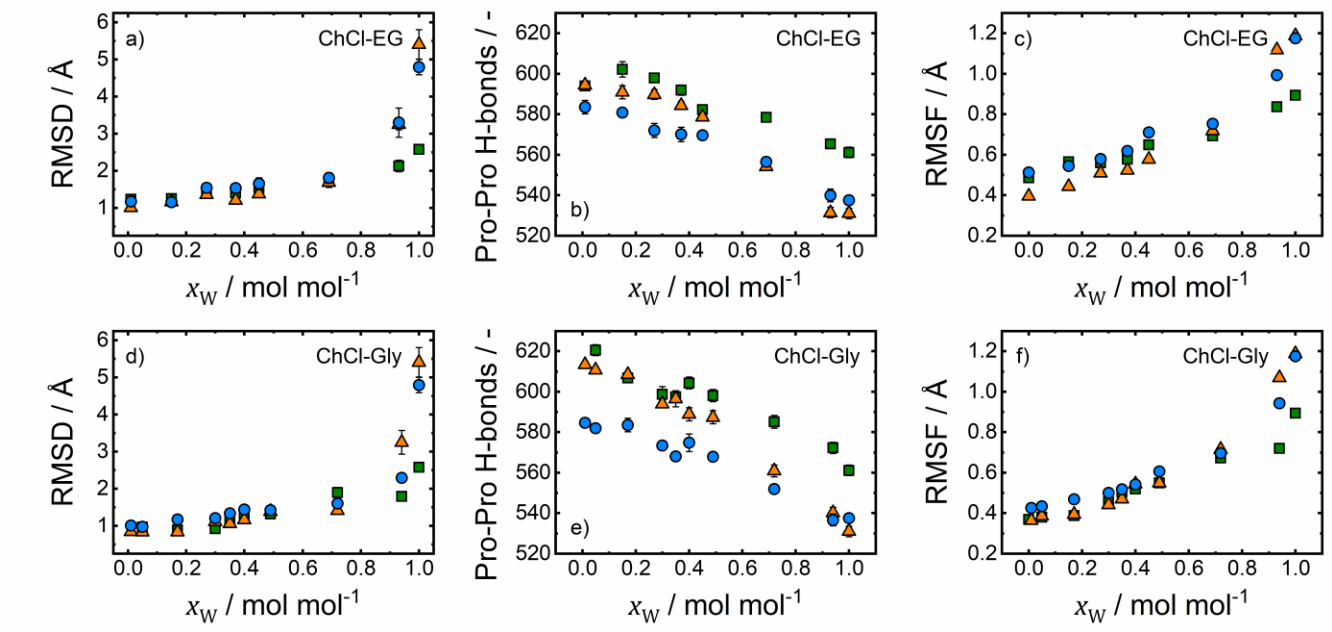


**Figure 10.** Structural properties of HLADH in mixtures of ChCl-EG (top) and ChCl-Gly (bottom) in dependency of the water mole fraction $x_W$ at 298 K and 1 bar. Left: Time averages of the root mean square deviations of the $C_\alpha$ atoms of HLADH with respect to the PDB structure (PDB entry 6O91[80]) for the last 40 ns of the trajectory. The error bars indicate 95 % confidence intervals of block averages with a block size of 5 ns. Middle: Time averages of intra-protein hydrogen bonds averaged over the last 40 ns seconds of the trajectory using a cut-off distance of 0.35 nm and a cut-off angle of 30°. The error bars indicate 95 % confidence intervals of block averages with a block size of 5 ns. Right: Root mean square fluctuations of the $C_\alpha$ atoms of HLADH averaged over the last 40 ns and both protein chains. Blue circles: GAFF-DES[16] / Amber03*,[55] green squares: OPLS-DES[18] / OPLS-AA/M[60] and orange triangles: CGenFF[46,47] / CHARMM36m.[50]

concentrations below 50 mol% but agrees with GAFF-DES /Amber03* for larger water contents. In general, the deviations between the three force fields are comparably low with a maximum of 2%.

In case of the RMSF of HLADH in the DES/water mixtures (Figure 10c+f) a similar trend compared to the RMSD can be observed. The enzyme is much more rigid in highly concentrated DES solutions in comparison to the aqueous environment. This behavior of the enzyme is not special for these DESs, as a less flexible enzyme structure could also be observed in the studies of enzymes in organic solvents[43,44] and in a recent investigation of lipase in ChCl+urea.[39] Kumari et al.,[40] on the other hand, observed an increase in the flexibility of lysoenzyme in ChCl+urea/water mixture compared to the pure aqueous case. Similar to the RMSD, the largest differences in the RMSF between the three force fields occur for large water concentrations, where OPLS-DES/OPLS-AA/M predicts a much lower flexibility of HLADH. The small differences in the enzyme flexibility at low water content may be explained by the diverging representation of the dynamic viscosity. For instance, CGenFF overestimates the viscosity of low water solutions, which resulted in a less flexible enzyme structure in the corresponding simulations. GAFF-DES, on the other side, estimating the lowest dynamic viscosity of the tested force fields led to a more flexible enzyme in the simulations.

Although the combination of the OPLS-DES force field for ChCl-Gly and TIP3P representing water led to a formation of a second glycerol phase, the structural behavior of HLADH seems to be mostly unaffected by this phase separation. Instead, the RMSD, intra-protein hydrogen bond and RMSF in the simulations of OPLS-DES/OPLS-AA/M mostly agree with the description of HLADH in the DES/water mixtures by CGenFF/CHARMM36m and GAFF-DES/Amber03*. This might be explained by the location of HLADH in the simulations of HLADH using OPLS-DES, where a phase separation occurred. The enzyme is located at the interface of the glycerol and ChCl/water phases. Thereby, its main volume is incorporated in the ChCl/water phase. Nevertheless, some part of the enzyme is still in contact with the glycerol phase. The location of HLADH in the simulations combined with its structural properties suggests, that ChCl has a much larger impact on HLADH's conformation in the DES solutions compared to glycerol. In case of large water contents, however, the values for OPLS-DES/OPLS-AA/M diverge from the other to force fields. Since it is also the case in the pure aqueous environment, this effect might be caused by the OPLS-AA/M force field and not affected by the representation of the DESs by OPLS-DES.

### Enzyme-solvent interactions

In addition to the structural behavior of HLADH in the DES/water mixtures, the interactions between enzyme and solvent molecules are of particular importance to understand the catalytic performance of HLADH in these environments. For instance, a sufficient hydration of HLADH is essential for its bioactivity.[41] Although some enzyme-bound water has to be preserved, the rest of the "bulk" water can in theory be replaced by an organic solvent or DES.[45] While the experimental determination of the hydration levels of enzymes is difficult, its computation from MD simulations is rather straight forward. Therefore, and due to their importance, the hydration and solvation layers of HLADH in the investigated solutions were compared for the different force fields.

Figure 11 shows the hydration layer of HLADH in the simulations with ChCl-EG and ChCl-Gly in dependency on the water content. A water molecule is thereby defined to be in the

hydration layer, if its oxygen is within 3.5 Å of any non-hydrogen protein atom.[43,106] This corresponds to the end of the first peak in radial distribution functions around the enzyme. At water concentrations below 50 mol% all three force fields give comparable values for the hydration layer of HLADH in ChCl-EG and ChCl-Gly with the largest discrepancy occurring for OPLS-DES at 40 mol% in ChCl-Gly. This means that although the liquid structure of ChCl-Gly in OPLS-DES is not reflected correctly, the hydration layer is represented in agreement with the other force fields. Above 50 mol% of water, the hydration layers show small differences, where CGenFF/CHARMM36m predict a larger hydration than the other force fields. In analogy to the structural data, the hydration layer in pure water that is computed by OPLS-AA/M disagrees with the hydration layer from CHARMM36m and Amber03*. This effect might be caused by a difference in the conformation of HLADH in aqueous simulations as indicated by Figure 10.

Although the OPLS-DES force field leads to a cluster formation with increasing water concentrations, the interaction of HLADH with water seems to be mostly unaffected by these clusters in particular for low water contents. As discussed above, HLADH is mainly located in the ChCl/water phase. The similar hydration of HLADH in the OPLS-DES simulations compared to the other force fields might be caused by two contrasting effects. The concentration of water is larger in the ChCl/water phase compared to the total concentration, while the surface of HLADH in contact with the aqueous phase is reduced, as some amount of HLADH is in direct contact with the glycerol phase. In addition, the interaction between water and the protein is rather unique as water was the only solvent that could diffuse into the enzyme structure contrary to glycerol and choline chloride. This also means, that the conclusions of an earlier publication[41] about the behavior of HLADH in ChCl-Gly/water mixtures using OPLS-DES/OPLS-AA/M as force field could be confirmed by the simulations performed using GAFF-DES/Amber03* as well as CGenFF/ CHARMM36m.

Besides the hydration layer, the interactions of HLADH with the DES components are of particular interest in order to find a suitable reaction environment for the enzyme. Figure 12 shows the solvation layers of choline (Figure 12a+d), chloride (Figure 12b+e) and the HBD (Figure 12c+f) in dependency of the water content. In analogy to water, a chloride ion is considered in the solvation layer, if it is within a distance of 3.5 Å of any non-hydrogen atom of the protein. Due to the larger size of the choline and HBD molecules, a different cut-off for the solvation layer had to be chosen. The decision of these cut-off distances is based on radial distribution of the solvent around the enzyme. Choline is considered in the solvation layer, if its central carbon (CN4) is within 6 Å of a heavy protein atom. For glycerol the cut-off is 5 Å and based on the central carbon (CG2), for ethylene glycol 4 Å and based on the carbon CE1.

The solvation layer of choline (Figure 12a+d) displays a nearly linear decrease in ChCl-EG as well as ChCl-Gly. Though, the number of choline molecules on HLADH's surface in ChCl-EG are by up to 60 molecules larger compared to ChCl-Gly. All three force fields give quantitively agreeing results with the exception of OPLS-DES/OPLS-AA/M for ChCl-Gly (Figure 12d). Figure 12b+e depicts a similar linear decrease for chloride with quantitative discrepancies between the three force fields. OPLS-DES/OPLS-AA/M give the largest solvation layer of chloride by starting from ~200 molecules in case of the pure DESs followed by CGenFF/CHARMM36m (~150 for ChCl-EG, ~130 for ChCl-Gly). The combination of GAFF-DES and Amber03* predict, on the other side, a much lower chloride solvation with ~100 and ~80 chloride molecules for ChCl-EG and ChCl-Gly, respectively. These quantitative differences diminish for increasing water contents.

Figure 12c+f reveal an unusual dependency of the solvation layer of HBD (either glycerol or ethylene glycol). In contrast to choline or chloride, the solvation layers of the HBD do not decrease but stay almost constant when the concentration of water is raised up to 50 mol%. This indicates a high affinity of HLADH towards interacting with glycerol and ethylene glycol. Starting between 50 mol% and 70 mol% the amounts of HBD on HLADH's surface is then drastically reduced. With the exception of ChCl-Gly computed by OPLS-DES/OPLS-AA/M, the three tested force fields give similar trends for the HBD solvation that are consistent with the other solvation layers. In CGenFF/CHARMM36m and OPLS-DES/OPLS-AA/M the interactions with chloride are slightly preferred over the HBD, whereas GAFF-DES/Amber03* shows a higher affinity towards the HBD. The description of OPLS-DES/OPLS-AA/M differs from this trend and shows a much lower solvation of glycerol with large fluctuations occurring between the concentrations.

As already discussed, the combination of OPLS-DES and a water force field resulted in a formation of glycerol clusters and subsequently into phase separation. This effect is clearly visible in the solvation data provided in Figure 12d-f, as the solvation layers for OPLS-DES/OPLS-AA/M in ChCl-Gly significantly differ from the description of the other force fields. They suggest that the protein is in closer contact to choline and chloride than to glycerol, which could be confirmed by visual inspection. Interestingly, the interaction sites of glycerol seem to be replaced by choline chloride in the ChCl/water phase. This consequently resulted in a similar hydration of HLADH compared to the other force fields despite phase separation. The arrangement of the enzyme in the ChCl/water phase can explain the discrepancies for OPLS-DES observed in ChCl-Gly. On the other hand, the solvation with water (Figure 11b) remained unchanged.

GAFF-DES and OPLS-DES have introduced charge scaling of different components of the DES in order to improve the dynamic behavior of the DESs in MD simulations. These reduced charges can, on the other hand, impact the interaction of the DES with a biomolecule e.g., their capabilities to form hydrogen bonds. Excluding the data of the ChCl-Gly/water mixtures using OPLS-DES, that are clearly influenced by the phase separation, the solvation layers indicate that the charge scaling has a diminishing impact on the enzyme-solvent interactions for the tested systems. A charge scaling factor of 0.8 and 0.9 applied to choline in OPLS-DES and GAFF-DES, respectively, did not influence its interaction with HLADH in the simulations, as all three force fields gave similar solvation layers of choline. The interaction with the HBDs (glycerol and ethylene glycol) are preferred in the simulations using GAFF-DES. However, OPLS-DES (partial charges scaled by 0.8) and CGenFF (no charge scaling) give a similar number of ethylene glycol molecules in direct contact with the enzyme, which is suggesting that the non-bonded LJ-parameters have a larger impact on the enzyme-solvent interactions. This is supported by the ordering of the solvation layers of chloride, as it does not reflect the amount of applied charge scaling in the respective force fields. On the other side, the LJ-well-depth $\varepsilon_{LJ}$ of chloride ions is much

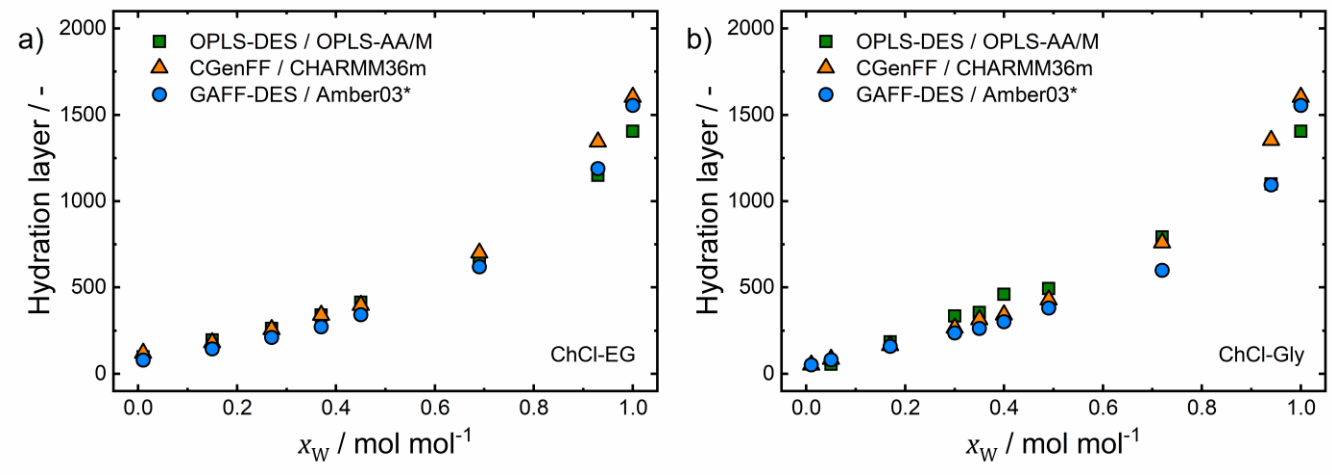


**Figure 11.** Time averages of the hydration layer of HLADH in mixtures of ChCl-EG (a) and ChCl-Gly (b) in dependency of the water mole fraction $x_W$ from molecular dynamics simulations at 298 K and 1 bar. Water is considered to be in the hydration layer when its oxygen atom is within 3.5 Å of any non-hydrogen atom of HLADH. The error bars indicate 95 % confidence intervals of block averages for the last 40 ns of the trajectory with a block size of 5 ns and are smaller than the symbol size. Blue circles: GAFF-DES[16] / Amber03*,[55] green squares: OPLS-DES[18] / OPLS-AA/M[60] and orange triangles: CGenFF[46,47] / CHARMM36m.[50]

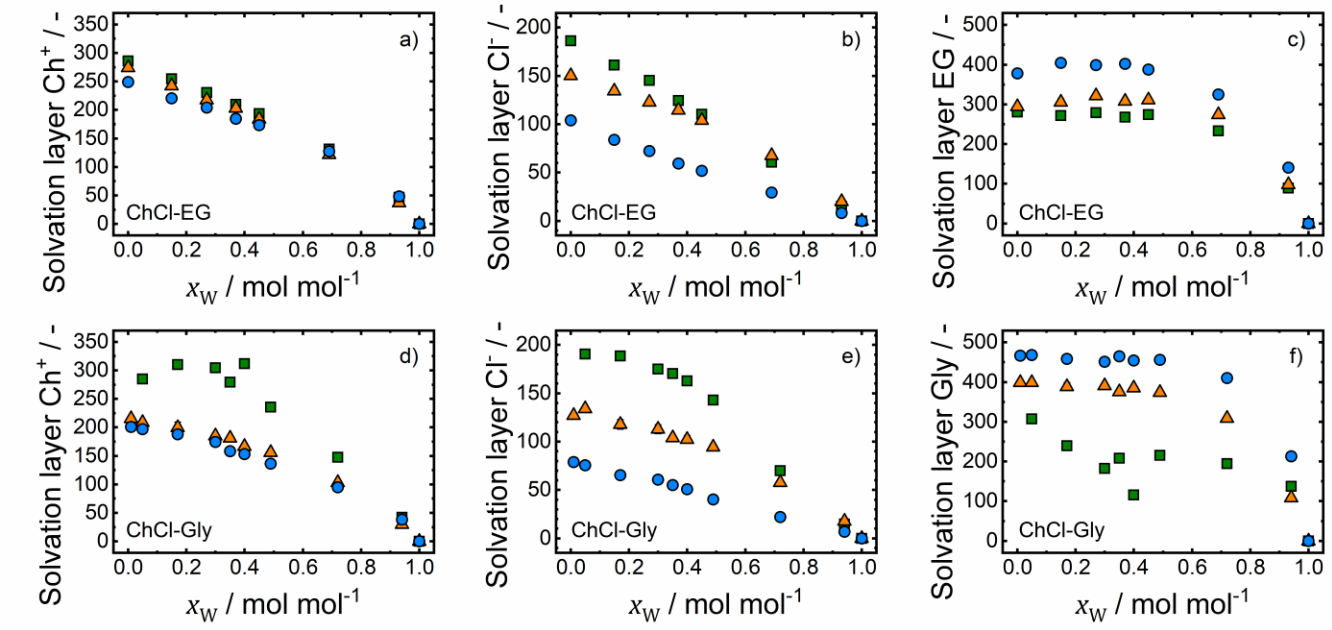


**Figure 12.** Time averages of the solvation layers of HLADH in mixtures of ChCl-EG (top) and ChCl-Gly (bottom) in dependency of the water mole fraction $x_W$ from molecular dynamics simulations at 298 K and 1 bar. The error bars indicate 95 % confidence intervals of block averages for the last 40 ns of the trajectory with a block size of 5 ns and are smaller than the symbol size. Left: Choline is considered to be in the solvation layer when its central carbon (CN4) is within 6 Å of any non-hydrogen of HLADH. Middle: Chloride ions within 3.5 Å of any non-hydrogen atom of HLADH are considered to be in the solvation layer. Right: Glycerol is considered to be in the solvation layer when its central carbon (CG2) is within 5 Å and ethylene glycol is considered in the solvation layer when the carbon atom CE1 is within 4 Å of any non-hydrogen atom of HLADH. Blue circles: GAFF-DES[16] / Amber03*,[55] green squares: OPLS-DES[18] / OPLS-AA/M[60] and orange triangles: CGenFF[46,47] / CHARMM36m.[50]

smaller in GAFF-DES ($\varepsilon_{LJ} = 0.418$ kJ mol$^{-1}$) compared to the other force fields (OPLS-DES: 0.619 kJ mol$^{-1}$, CGenFF: 0.628 kJ mol$^{-1}$), which contributes to the observation of fewer chloride ions in the solvation layer.

In conclusion, CGenFF/CHARMM36m and GAFF-DES/Amber03* show a similar and consistent behavior for the solvation layer with the latter favoring the HBD and CGenFF/CHARMM36m favoring the chloride ion. Up to 50 mol% the additional water in the system replaces choline and chloride on the surface of HLADH. Surprisingly, the number of glycerol and ethylene glycol molecules stays constant until roughly 50 mol%. Afterwards, the HBD is also replaced on the surface by water molecules. This indicates a preferred interaction of the enzyme with the HBD. Its implications on the biocatalytic performance of HLADH, however, remain to be investigated in the future. The solvation data show, that the OPLS-

DES force field is not suitable to elucidate the behavior of HLADH in the DES composed of choline chloride and glycerol.

## Conclusions

The force field comparison within this work could reveal strengths and weaknesses of different DESs force fields using the liquid density $\rho$, thermodynamic water activity $a_W$ and dynamic viscosity $\eta$ for validation. The static and dynamic properties for low water concentrations (< 40 mol%) are best reproduced by the GAFF-DES[16,17] force field. However, for larger water concentrations (> 50 mol%) CGenFF[46,47] and to some extend also OPLS-DES[18] (for ChCl-EG) reproduce the water activity in better agreement with the experimental data, while also correctly reflecting the viscosity. An in-depth analysis of characteristic radial distribution functions and hydrogen bonds within the DES uncovered an unusual formation of glycerol clusters with increasing water content in the simulations of ChCl-Gly using OPLS-DES. Since this effect was neither seen in the experiment nor present for the other tested force fields, we conclude that OPLS-DES[18] is not a suitable interaction model for ChCl-Gly/water mixtures.

The observed phase separation for ChCl-Gly by OPLS-DES did not significantly influence the structure of HLADH in the MD simulations. All three tested force field combinations predict a similar rigid structure of HLADH in the DES mixtures at low water contents, that is closer to the crystallographic structure (PDB entry 6O91) than in an aqueous environment. The largest deviation in the enzyme structure were observed for the pure aqueous case and can be attributed to the protein force fields.[105] While the force field artifact within OPLS-DES did not affect the structure of HLADH as well as its hydration layer, which could confirm the conclusions form an earlier publication,[41] it led to a different interaction with the DESs. The implications of the structural behavior of HLADH as well as the solvation effects of the DESs, that are observed in the MD simulations within this work, on the catalytic performance of the enzyme are yet to be shown.

Furthermore, we investigated the influence of the acceleration amplitude on the viscosity calculations. For high amplitudes we found decreasing viscosities, which is an indication of a distortion of the equilibrium. For very low amplitudes the result is fluctuating. However, in between these two regimes there is a range for which the result is independent of the amplitude and as such being the region of interest.

In summary, in most cases the force fields gave similar results. However, the observed differences can guide the choice of the suitable force field. The OPLS-DES[18] cannot be recommended to be used for ChCl-Gly/water mixtures, due to the observed phase separation. The CGenFF[46,47] was the only tested force field that was not optimized for DES, which results in large deviation for the viscosity at low water concentrations. Especially, due to the findings for the water activity and the viscosity, the GAFF-DES[16] force field seems to be preferential for $x_W < 0.5$, while CGenFF[46,47] outperformed the other force fields for larger water concentrations. For enzyme simulations in DES water mixtures the most notable difference was observed in the number of chloride ions and HBD in the solvation layer. Unfortunately, a lack of suitable experimental data prevents the usage of this data as selection criterion.

## ASSOCIATED CONTENT

### Supporting Information

The Supporting Information is available free of charge on the ACS Publications website.

The Supporting Information contains one PDF file including the compositions of the DES/water mixtures in the MD simulations (Tables S1, S2, S3, S4 and S5), TI curves for the determination of $\Delta G_W^{solv}$ (Figure S1), dynamic viscosities $\eta$ in dependency of the chosen amplitude $\mathcal{A}$ (Figure S2), parity plot for error estimates of $\eta$ (Figure S3), dynamic viscosities $\eta$ for CGenFF (scaled) (Figure S4), adjusted glycerol dihedrals for OPLS-DES[98,99] (Table S6) and its impact on the dynamic viscosity of ChCl-Gly (Figure S5), mean square displacements of chloride (Figure S6), snapshots of MD simulations of ChCl-Gly/water mixtures (Figure S7), comparison of RMSD and RMSF with Huang et al.[41] (Figure S8) and the radius of gyration of HLADH (Figure S9).

## AUTHOR INFORMATION


### Corresponding Author

* Sven Jakobtorweihen (E-mail: *jakobtorweihen@tuhh.de*)


### Notes

The authors declare no competing financial interest.

## ACKNOWLEDGMENT


We want to gratefully thank Maria Alejandra Tibaquira Martinez for the support with the solvation free energy calculations. We thank Niels Hansen for sharing some force fields files in GROMACS format. This work was financially supported by Deutsche Forschungsgemeinschaft (DFG) grant nos. KA 4399/3-1 and JA 2500/5-1; jointly acquired project. Computational resources for the MD simulations of this work have been provided by the North-German Supercomputing Alliance (HLRN).


## ABBREVIATIONS

DESs, deep eutectic solvents; ChCl, choline chloride; HBA, hydrogen bond acceptor; HBD, hydrogen bond donor; ChCl-Gly, choline chloride – glycerol (molar ratio 1:2); ChCl-EG, choline chloride – ethylene glycol (molar ratio 1:2); MD, molecular dynamics; ILs, ionic liquids; EMD, equilibrium molecular dynamics; NEMD, non-equilibrium molecular dynamics; CHARMM, Chemistry at Harvard Macromolecular Mechanics; CGenFF, CHARMM general force field; GAFF, General Amber force field; OPLS-AA, Optimized Potential for Liquid Simulations – All Atom; HLADH, horse liver alcohol dehydrogenase; TIP3P, Three-site transferrable intermolecular potential; TIP4P, Four-site transferrable intermolecular potential; TIP5P, Five-site transferrable intermolecular potential; SPC/E, extended simple point charge model; LINCS, Linear Constraint Solver; PME, Particle-Mesh Ewald summation; RDFs, radial distribution functions; PDB, Protein Data Base; NPT, isobaric-isothermal ensemble; NVT, canonical ensemble; CALB, *Candida antarctica* lipase B; $O_{Ch}$, oxygen of choline; $O_{EG}$, oxygen of ethylene glycol, $O_{Gly}$, oxygen of glycerol; Cl, chloride ion; Ch, choline; Gly, glycerol; EG, ethylene glycol; RMSD, root mean square deviations; RMSF, root mean square fluctuations.

## REFERENCES


(1) Wohlgemuth, R. Biocatalysis—Key to Sustainable Industrial Chemistry. *Curr. Opin. Biotechnol.* **2010**, *21* (6), 713–724. https://doi.org/10.1016/j.copbio.2010.09.016.

(2) Ma, Y.; Li, P.; Li, Y.; Willot, S. J. -P.; Zhang, W.; Ribitsch, D.; Choi, Y. H.; Verpoorte, R.; Zhang, T.; Hollmann, F.; Wang, Y.

Natural Deep Eutectic Solvents as Multifunctional Media for the Valorization of Agricultural Wastes. *ChemSusChem* **2019**, *12* (7), 1310–1315. https://doi.org/10.1002/cssc.201900043.

(3) Pätzold, M.; Siebenhaller, S.; Kara, S.; Liese, A.; Syldatk, C.; Holtmann, D. Deep Eutectic Solvents as Efficient Solvents in Biocatalysis. *Trends Biotechnol.* **2019**, *37* (9), 943–959. https://doi.org/10.1016/j.tibtech.2019.03.007.

(4) Marcus, Y. *Deep Eutectic Solvents*, 1st ed.; Springer International Publishing: Switzerland, 2019. https://doi.org/10.1007/978-3-030-00608-2.

(5) Hollenbach, R.; Ochsenreither, K.; Syldatk, C. Enzymatic Synthesis of Glucose Monodecanoate in a Hydrophobic Deep Eutectic Solvent. *Int. J. Mol. Sci.* **2020**, *21* (12), 4342. https://doi.org/10.3390/ijms21124342.

(6) Hansen, B. B.; Spittle, S.; Chen, B.; Poe, D.; Zhang, Y.; Klein, J. M.; Horton, A.; Adhikari, L.; Zelovich, T.; Doherty, B. W.; Gurkan, B.; Maginn, E. J.; Ragauskas, A.; Dadmun, M.; Zawodzinski, T. A.; Baker, G. A.; Tuckerman, M. E.; Savinell, R. F.; Sangoro, J. R. Deep Eutectic Solvents: A Review of Fundamentals and Applications. *Chem. Rev.* **2021**, *121* (3), 1232–1285. https://doi.org/10.1021/acs.chemrev.0c00385.

(7) Kist, J. A.; Zhao, H.; Mitchell-Koch, K. R.; Baker, G. A. The Study and Application of Biomolecules in Deep Eutectic Solvents. *J. Mater. Chem. B* **2021**, *9* (3), 536–566. https://doi.org/10.1039/D0TB01656J.

(8) Erol, Ö.; Hollmann, F. Natural Deep Eutectic Solvents as Performance Additives for Biocatalysis. In *Advances in Botanical Research*; Elsevier, 2021; Vol. 97, pp 95–132. https://doi.org/10.1016/bs.abr.2020.09.004.

(9) Alonso, D. A.; Baeza, A.; Chinchilla, R.; Guillena, G.; Pastor, I. M.; Ramón, D. J. Deep Eutectic Solvents: The Organic Reaction Medium of the Century. *Eur. J. Org. Chem.* **2016**, *2016* (4), 612–632. https://doi.org/10.1002/ejoc.201501197.

(10) Abbott, A. P.; Capper, G.; Davies, D. L.; Rasheed, R. K.; Tambyrajah, V. Novel Solvent Properties of Choline Chloride/Urea MixturesElectronic Supplementary Information (ESI) Available: Spectroscopic Data. See Http://Www.Rsc.Org/Suppdata/Cc/B2/B210714g/. *Chem. Commun.* **2003**, No. 1, 70–71. https://doi.org/10/cw673s.

(11) Martins, M. A. R.; Pinho, S. P.; Coutinho, J. A. P. Insights into the Nature of Eutectic and Deep Eutectic Mixtures. *J. Solut. Chem.* **2019**, *48* (7), 962–982. https://doi.org/10.1007/s10953-018-0793-1.

(12) Abbott, A. P.; Cullis, P. M.; Gibson, M. J.; Harris, R. C.; Raven, E. Extraction of Glycerol from Biodiesel into a Eutectic Based Ionic Liquid. *Green Chem.* **2007**, *9* (8), 868. https://doi.org/10.1039/b702833d.

(13) Guajardo, N.; Müller, C. R.; Schrebler, R.; Carlesi, C.; Domínguez de María, P. Deep Eutectic Solvents for Organocatalysis, Biotransformations, and Multistep Organocatalyst/Enzyme Combinations. *ChemCatChem* **2016**, *8* (6), 1020–1027. https://doi.org/10.1002/cctc.201501133.

(14) Juneidi, I.; Hayyan, M.; Hashim, M. A. Intensification of Biotransformations Using Deep Eutectic Solvents: Overview and Outlook. *Process Biochem.* **2018**, *66*, 33–60. https://doi.org/10.1016/j.procbio.2017.12.003.

(15) Gorke, J. T.; Srienc, F.; Kazlauskas, R. J. Hydrolase-Catalyzed Biotransformations in Deep Eutectic Solvents. *Chem. Commun.* **2008**, No. 10, 1235. https://doi.org/10.1039/b716317g.

(16) Perkins, S. L.; Painter, P.; Colina, C. M. Experimental and Computational Studies of Choline Chloride-Based Deep Eutectic Solvents. *J. Chem. Eng. Data* **2014**, *59* (11), 3652–3662. https://doi.org/10.1021/je500520h.

(17) Perkins, S. L.; Painter, P.; Colina, C. M. Molecular Dynamic Simulations and Vibrational Analysis of an Ionic Liquid Analogue. *J. Phys. Chem. B* **2013**, *117* (35), 10250–10260. https://doi.org/10.1021/jp404619x.

(18) Doherty, B.; Acevedo, O. OPLS Force Field for Choline Chloride-Based Deep Eutectic Solvents. *J. Phys. Chem. B* **2018**, *122* (43), 9982–9993. https://doi.org/10.1021/acs.jpcb.8b06647.

(19) Mainberger, S.; Kindlein, M.; Bezold, F.; Elts, E.; Minceva, M.; Briesen, H. Deep Eutectic Solvent Formation: A Structural View Using Molecular Dynamics Simulations with Classical Force Fields. *Mol. Phys.* **2017**, *115* (9–12), 1309–1321. https://doi.org/10.1080/00268976.2017.1288936.

(20) Ferreira, E. S. C.; Voroshylova, I. V.; Pereira, C. M.; D. S. Cordeiro, M. N. Improved Force Field Model for the Deep Eutectic Solvent Ethaline: Reliable Physicochemical Properties. *J. Phys. Chem. B* **2016**, *120* (38), 10124–10137. https://doi.org/10.1021/acs.jpcb.6b07233.

(21) García, G.; Atilhan, M.; Aparicio, S. The Impact of Charges in Force Field Parameterization for Molecular Dynamics Simulations of Deep Eutectic Solvents. *J. Mol. Liq.* **2015**, *211*, 506–514. https://doi.org/10/f7z3x8.

(22) González de Castilla, A.; Bittner, J. P.; Müller, S.; Jakobtorweihen, S.; Smirnova, I. Thermodynamic and Transport Properties Modeling of Deep Eutectic Solvents: A Review on GE-Models, Equations of State, and Molecular Dynamics. *J. Chem. Eng. Data* **2020**, *65* (3), 943–967. https://doi.org/10.1021/acs.jced.9b00548.

(23) Bhargava, B. L.; Balasubramanian, S. Refined Potential Model for Atomistic Simulations of Ionic Liquid [Bmim][PF6]. *J. Chem. Phys.* **2007**, *127* (11), 114510. https://doi.org/10.1063/1.2772268.

(24) Zhang, Y.; Maginn, E. J. A Simple AIMD Approach to Derive Atomic Charges for Condensed Phase Simulation of Ionic Liquids. *J. Phys. Chem. B* **2012**, *116* (33), 10036–10048. https://doi.org/10.1021/jp3037999.

(25) Youngs, T. G. A.; Hardacre, C. Application of Static Charge Transfer within an Ionic-Liquid Force Field and Its Effect on Structure and Dynamics. *ChemPhysChem* **2008**, *9* (11), 1548–1558. https://doi.org/10.1002/cphc.200800200.

(26) Wendler, K.; Zahn, S.; Dommert, F.; Berger, R.; Holm, C.; Kirchner, B.; Delle Site, L. Locality and Fluctuations: Trends in Imidazolium-Based Ionic Liquids and Beyond. *J. Chem. Theory Comput.* **2011**, *7* (10), 3040–3044. https://doi.org/10.1021/ct200375v.

(27) Zahn, S.; Kirchner, B.; Mollenhauer, D. Charge Spreading in Deep Eutectic Solvents. *ChemPhysChem* **2016**, *17* (21), 3354–3358. https://doi.org/10/f3rbtj.

(28) Chaumont, A.; Engler, E.; Schurhammer, R. Is Charge Scaling Really Mandatory When Developing Fixed-Charge Atomistic Force Fields for Deep Eutectic Solvents? *J Phys Chem B* **2020**, *124* (33), 7239–7250.

(29) Zhekenov, T.; Toksanbayev, N.; Kazakbayeva, Z.; Shah, D.; Mjalli, F. S. Formation of Type III Deep Eutectic Solvents and Effect of Water on Their Intermolecular Interactions. *Fluid Phase Equilibria* **2017**, *441*, 43–48. https://doi.org/10.1016/j.fluid.2017.01.022.

(30) Ahmadi, R.; Hemmateenejad, B.; Safavi, A.; Shojaeifard, Z.; Shahsavar, A.; Mohajeri, A.; Heydari Dokoohaki, M.; Zolghadr, A. R. Deep Eutectic–Water Binary Solvent Associations Investigated by Vibrational Spectroscopy and Chemometrics. *Phys. Chem. Chem. Phys.* **2018**, *20* (27), 18463–18473. https://doi.org/10.1039/C8CP00409A.

(31) Weng, L.; Toner, M. Janus-Faced Role of Water in Defining Nanostructure of Choline Chloride/Glycerol Deep Eutectic Solvent. *Phys. Chem. Chem. Phys.* **2018**, *20* (35), 22455–22462. https://doi.org/10.1039/C8CP03882A.

(32) Shah, D.; Mjalli, F. S. Effect of Water on the Thermo-Physical Properties of Reline: An Experimental and Molecular Simulation Based Approach. *Phys Chem Chem Phys* **2014**, *16* (43), 23900–23907. https://doi.org/10/gc9256.

(33) Bedrov, D.; Piquemal, J.-P.; Borodin, O.; MacKerell, A. D.; Roux, B.; Schröder, C. Molecular Dynamics Simulations of Ionic Liquids and Electrolytes Using Polarizable Force Fields. *Chem. Rev.* **2019**, *119* (13), 7940–7995. https://doi.org/10.1021/acs.chemrev.8b00763.

(34) Hess, B. Determining the Shear Viscosity of Model Liquids from Molecular Dynamics Simulations. *J. Chem. Phys.* **2002**, *116* (1), 209. https://doi.org/10.1063/1.1421362.

(35) Maginn, E. J.; Messerly, R. A.; Carlson, D. J.; Roe, D. R.; Elliott, J. R. Best Practices for Computing Transport Properties 1. Self-Diffusivity and Viscosity from Equilibrium Molecular Dynamics [Article v1.0]. *Living J. Comput. Mol. Sci.* **2019**, *1* (1), 6324. https://doi.org/10.33011/livecoms.1.1.6324.

(36) Nieto-Draghi, C.; Fayet, G.; Creton, B.; Rozanska, X.; Rotureau, P.; de Hemptinne, J.-C.; Ungerer, P.; Rousseau, B.; Adamo, C.

A General Guidebook for the Theoretical Prediction of Physicochemical Properties of Chemicals for Regulatory Purposes. *Chem. Rev.* **2015**, *115* (24), 13093–13164. https://doi.org/10.1021/acs.chemrev.5b00215.

(37) Ciccotti, G.; Jacucci, G.; McDonald, I. R. Thought-Experiments by Molecular Dynamics. *J. Stat. Phys.* **1979**, *21* (1), 1–22. https://doi.org/10.1007/BF01011477.

(38) Baz, J.; Held, C.; Pleiss, J.; Hansen, N. Thermophysical Properties of Glyceline-Water Mixtures Investigated by Molecular Modelling. *Phys. Chem. Chem. Phys.* **2019**, *21* (12), 6467–6476. https://doi.org/10.1039/C9CP00036D.

(39) Shehata, M.; Unlu, A.; Sezerman, U.; Timucin, E. Lipase and Water in a Deep Eutectic Solvent: Molecular Dynamics and Experimental Studies of the Effects of Water-In-Deep Eutectic Solvents on Lipase Stability. *J. Phys. Chem. B* **2020**, *124* (40), 8801–8810. https://doi.org/10.1021/acs.jpcb.0c07041.

(40) Kumari, P.; Kumari, M.; Kashyap, H. K. How Pure and Hydrated Reline Deep Eutectic Solvents Affect the Conformation and Stability of Lysozyme: Insights from Atomistic Molecular Dynamics Simulations. *J Phys Chem B* **2020**, *124*, 11919−11927.

(41) Huang, L.; Bittner, J. P.; María, P. D. de; Jakobtorweihen, S.; Kara, S. Modeling Alcohol Dehydrogenase Catalysis in Deep Eutectic Solvent/Water Mixtures. *ChemBioChem* **2020**, *21* (6), 811–817. https://doi.org/10.1002/cbic.201900624.

(42) Monhemi, H.; Housaindokht, M. R.; Moosavi-Movahedi, A. A.; Bozorgmehr, M. R. How a Protein Can Remain Stable in a Solvent with High Content of Urea: Insights from Molecular Dynamics Simulation of Candida Antarctica Lipase B in Urea : Choline Chloride Deep Eutectic Solvent. *Phys. Chem. Chem. Phys.* **2014**, *16* (28), 14882. https://doi.org/10.1039/c4cp00503a.

(43) Wedberg, R.; Abildskov, J.; Peters, G. H. Protein Dynamics in Organic Media at Varying Water Activity Studied by Molecular Dynamics Simulation. *J. Phys. Chem. B* **2012**, *116* (8), 2575–2585. https://doi.org/10.1021/jp211054u.

(44) Trodler, P.; Pleiss, J. Modeling Structure and Flexibility of Candida Antarctica Lipase B in Organic Solvents. *BMC Struct. Biol.* **2008**, *8* (1), 9. https://doi.org/10.1186/1472-6807-8-9.

(45) Zaks, A.; Klibanov, A. M. The Effect of Water on Enzyme Action in Organic Media. *J. Biol. Chem.* **1988**, *263* (17), 8017–8021.

(46) Vanommeslaeghe, K.; Hatcher, E.; Acharya, C.; Kundu, S.; Zhong, S.; Shim, J.; Darian, E.; Guvench, O.; Lopes, P.; Vorobyov, I.; Mackerell, A. D. CHARMM General Force Field: A Force Field for Drug-like Molecules Compatible with the CHARMM All-Atom Additive Biological Force Fields. *J. Comput. Chem.* **2010**, *31* (4), 671–690. https://doi.org/10.1002/jcc.21367.

(47) Yu, W.; He, X.; Vanommeslaeghe, K.; MacKerell, A. D. Extension of the CHARMM General Force Field to Sulfonyl-Containing Compounds and Its Utility in Biomolecular Simulations. *J. Comput. Chem.* **2012**, *33* (31), 2451–2468. https://doi.org/10.1002/jcc.23067.

(48) Kaur, S.; Shobhna; Kashyap, H. K. Insights Gained from Refined Force-Field for Pure and Aqueous Ethylene Glycol through Molecular Dynamics Simulations. *J. Phys. Chem. B* **2019**, *123* (30), 6543–6553. https://doi.org/10.1021/acs.jpcb.9b03950.

(49) Kaur, S.; Malik, A.; Kashyap, H. K. Anatomy of Microscopic Structure of Ethaline Deep Eutectic Solvent Decoded through Molecular Dynamics Simulations. *J. Phys. Chem. B* **2019**, *123* (39), 8291–8299. https://doi.org/10.1021/acs.jpcb.9b06624.

(50) Huang, J.; Rauscher, S.; Nawrocki, G.; Ran, T.; Feig, M.; de Groot, B. L.; Grubmüller, H.; MacKerell, A. D. CHARMM36m: An Improved Force Field for Folded and Intrinsically Disordered Proteins. *Nat. Methods* **2017**, *14* (1), 71–73. https://doi.org/10.1038/nmeth.4067.

(51) Humphrey, W.; Dalke, A.; Schulten, K. VMD: Visual Molecular Dynamics. *J. Mol. Graph.* **1996**, *14* (1), 33–38. https://doi.org/10.1016/0263-7855(96)00018-5.

(52) VMD - Visual Molecular Dynamics http://www.ks.uiuc.edu/Research/vmd/ (accessed 2021 -01 -27).

(53) Wang, J.; Wolf, R. M.; Caldwell, J. W.; Kollman, P. A.; Case, D. A. Development and Testing of a General Amber Force Field. *J. Comput. Chem.* **2004**, *25* (9), 1157–1174. https://doi.org/10.1002/jcc.20035.

(54) Zhang, Y.; Poe, D.; Heroux, L.; Squire, H.; Doherty, B. W.; Long, Z.; Dadmun, M.; Gurkan, B.; Tuckerman, M. E.; Maginn, E. J. Liquid Structure and Transport Properties of the Deep Eutectic Solvent Ethaline. *J. Phys. Chem. B* **2020**, *124* (25), 5251–5264. https://doi.org/10.1021/acs.jpcb.0c04058.

(55) Best, R. B.; Hummer, G. Optimized Molecular Dynamics Force Fields Applied to the Helix−Coil Transition of Polypeptides. *J. Phys. Chem. B* **2009**, *113* (26), 9004–9015. https://doi.org/10.1021/jp901540t.

(56) Acevedo, O. Deep eutectic solvent force field parameters (OPLS-DES) https://github.com/orlandoacevedo/DES (accessed 2019 -02 -27).

(57) Doherty, B.; Zhong, X.; Gathiaka, S.; Li, B.; Acevedo, O. Revisiting OPLS Force Field Parameters for Ionic Liquid Simulations. *J. Chem. Theory Comput.* **2017**, *13* (12), 6131–6145. https://doi.org/10.1021/acs.jctc.7b00520.

(58) Sambasivarao, S. V.; Acevedo, O. Development of OPLS-AA Force Field Parameters for 68 Unique Ionic Liquids. *J. Chem. Theory Comput.* **2009**, *5* (4), 1038–1050. https://doi.org/10.1021/ct900009a.

(59) Jorgensen, W. L.; Maxwell, D. S.; Tirado-Rives, J. Development and Testing of the OPLS All-Atom Force Field on Conformational Energetics and Properties of Organic Liquids. *J. Am. Chem. Soc.* **1996**, *118* (45), 11225–11236. https://doi.org/10.1021/ja9621760.

(60) Robertson, M. J.; Tirado-Rives, J.; Jorgensen, W. L. Improved Peptide and Protein Torsional Energetics with the OPLS-AA Force Field. *J. Chem. Theory Comput.* **2015**, *11* (7), 3499–3509. https://doi.org/10.1021/acs.jctc.5b00356.

(61) Jorgensen, W. L. OPLS-AA/M for Proteins http://zarbi.chem.yale.edu/oplsaam.html (accessed 2019 -03 -22).

(62) Zhong, X.; Velez, C.; Acevedo, O. Partial Charges Optimized by Genetic Algorithms for Deep Eutectic Solvent Simulations. *J. Chem. Theory Comput.* **2021**, *17* (5), 3078–3087. https://doi.org/10.1021/acs.jctc.1c00047.

(63) Jorgensen, W. L.; Chandrasekhar, J.; Madura, J. D.; Impey, R. W.; Klein, M. L. Comparison of Simple Potential Functions for Simulating Liquid Water. *J. Chem. Phys.* **1983**, *79* (2), 926–935. https://doi.org/10.1063/1.445869.

(64) MacKerell, A. D.; Bashford, D.; Bellott, M.; Dunbrack, R. L.; Evanseck, J. D.; Field, M. J.; Fischer, S.; Gao, J.; Guo, H.; Ha, S.; Joseph-McCarthy, D.; Kuchnir, L.; Kuczera, K.; Lau, F. T. K.; Mattos, C.; Michnick, S.; Ngo, T.; Nguyen, D. T.; Prodhom, B.; Reiher, W. E.; Roux, B.; Schlenkrich, M.; Smith, J. C.; Stote, R.; Straub, J.; Watanabe, M.; Wiórkiewicz-Kuczera, J.; Yin, D.; Karplus, M. All-Atom Empirical Potential for Molecular Modeling and Dynamics Studies of Proteins †. *J. Phys. Chem. B* **1998**, *102* (18), 3586–3616. https://doi.org/10.1021/jp973084f.

(65) Durell, S. R.; Brooks, B. R.; Ben-Naim, A. Solvent-Induced Forces between Two Hydrophilic Groups. *J. Phys. Chem.* **1994**, *98* (8), 2198–2202. https://doi.org/10.1021/j100059a038.

(66) Abraham, M. J.; Murtola, T.; Schulz, R.; Páll, S.; Smith, J. C.; Hess, B.; Lindahl, E. GROMACS: High Performance Molecular Simulations through Multi-Level Parallelism from Laptops to Supercomputers. *SoftwareX* **2015**, *1–2*, 19–25. https://doi.org/10.1016/j.softx.2015.06.001.

(67) Abraham, M. J.; van der Spoel, D.; Lindahl, E.; Hess, B.; and the GROMACS development team. *GROMACS User Manual Version 2019.4*; 2019.

(68) Bekker, H.; Berendsen, H.; Dijkstra, E.; Achterop, S.; Vondrumen, R.; Vanderspoel, D.; Sijbers, A.; Keegstra, H.; Renardus, M. GROMACS - A PARALLEL COMPUTER FOR MOLECULAR-DYNAMICS SIMULATIONS. In *Physics Computing 92*; DeGroot, R. A., Nadrchal, J., Eds.; World Scientific: Singapore, 1992; pp 252–256.

(69) Grossfield, A.; Patrone, P. N.; Roe, D. R.; Schultz, A. J.; Siderius, D.; Zuckerman, D. M. Best Practices for Quantification of Uncertainty and Sampling Quality in Molecular Simulations [Article v1.0]. *Living J. Comput. Mol. Sci.* **2019**, *1* (1), 5067. https://doi.org/10.33011/livecoms.1.1.5067.

(70) Larsen, G. S.; Lin, P.; Hart, K. E.; Colina, C. M. Molecular Simulations of PIM-1-like Polymers of Intrinsic Microporosity. *Macromolecules* **2011**, *44* (17), 6944–6951. https://doi.org/10.1021/ma200345v.

(71) Liu, H.; Maginn, E.; Visser, A. E.; Bridges, N. J.; Fox, E. B. Thermal and Transport Properties of Six Ionic Liquids: An Experimental and Molecular Dynamics Study. *Ind. Eng. Chem. Res.* **2012**, *51* (21), 7242–7254. https://doi.org/10.1021/ie300222a.

(72) Martínez, L.; Andrade, R.; Birgin, E. G.; Martínez, J. M. PACKMOL: A Package for Building Initial Configurations for Molecular Dynamics Simulations. *J. Comput. Chem.* **2009**, *30* (13), 2157–2164. https://doi.org/10.1002/jcc.21224.

(73) Hockney, R. W. Potential Calculation And Some Applications. *Methods Comput Phys* **1970**, *9*, 135–211.

(74) Bussi, G.; Donadio, D.; Parrinello, M. Canonical Sampling through Velocity Rescaling. *J. Chem. Phys.* **2007**, *126* (1), 014101. https://doi.org/10.1063/1.2408420.

(75) Hess, B.; Bekker, H.; Berendsen, H. J. C. LINCS: A Linear Constraint Solver for Molecular Simulations. *J. Comput. Chem.* **1997**, *18* (12), 10.

(76) Miyamoto, S.; Kollman, P. A. Settle: An Analytical Version of the SHAKE and RATTLE Algorithm for Rigid Water Models. *J. Comput. Chem.* **1992**, *13* (8), 952–962. https://doi.org/10.1002/jcc.540130805.

(77) Berendsen, H. J. C.; Postma, J. P. M.; van Gunsteren, W. F.; DiNola, A.; Haak, J. R. Molecular Dynamics with Coupling to an External Bath. *J. Chem. Phys.* **1984**, *81* (8), 3684–3690. https://doi.org/10.1063/1.448118.

(78) Parrinello, M.; Rahman, A. Polymorphic Transitions in Single Crystals: A New Molecular Dynamics Method. *J. Appl. Phys.* **1981**, *52* (12), 7182–7190. https://doi.org/10.1063/1.328693.

(79) Darden, T.; York, D.; Pedersen, L. Particle Mesh Ewald: An $N \cdot \log(N)$ Method for Ewald Sums in Large Systems. *J. Chem. Phys.* **1993**, *98* (12), 10089–10092. https://doi.org/10.1063/1.464397.

(80) Kim, K.; Plapp, B. V. Substitutions of Amino Acid Residues in the Substrate Binding Site of Horse Liver Alcohol Dehydrogenase Have Small Effects on the Structures but Significantly Affect Catalysis of Hydrogen Transfer. *Biochemistry* **2020**, *59* (7), 862–879. https://doi.org/10.1021/acs.biochem.9b01074.

(81) Klimovich, P. V.; Shirts, M. R.; Mobley, D. L. Guidelines for the Analysis of Free Energy Calculations. *J. Comput. Aided Mol. Des.* **2015**, *29* (5), 397–411. https://doi.org/10.1007/s10822-015-9840-9.

(82) Kirkwood, J. G. Statistical Mechanics of Fluid Mixtures. *J. Chem. Phys.* **1935**, *3* (5), 300–313. https://doi.org/10.1063/1.1749657.

(83) Paliwal, H.; Shirts, M. R. A Benchmark Test Set for Alchemical Free Energy Transformations and Its Use to Quantify Error in Common Free Energy Methods. *J. Chem. Theory Comput.* **2011**, *7* (12), 4115–4134. https://doi.org/10.1021/ct2003995.

(84) Raabe, G. *Molecular Simulation Studies on Thermophysical Properties*, 1st ed.; Maginn, E., Ed.; Molecular Modeling and Simulation; Springer Singapore: Singapore, 2017. https://doi.org/10.1007/978-981-10-3545-6.

(85) Feenstra, K. A.; Hess, B.; Berendsen, H. J. C. Improving Efficiency of Large Time-Scale Molecular Dynamics Simulations of Hydrogen-Rich Systems. *J. Comput. Chem.* **1999**, *20* (8), 786–798. https://doi.org/10.1002/(SICI)1096-987X(199906)20:8<786::AID-JCC5>3.0.CO;2-B.

(86) Song, Y.; Dai, L. L. The Shear Viscosities of Common Water Models by Non-Equilibrium Molecular Dynamics Simulations. *Mol. Simul.* **2010**, *36* (7–8), 560–567. https://doi.org/10.1080/08927021003720553.

(87) Zhao, L.; Wang, X.; Wang, L.; Sun, H. Prediction of Shear Viscosities Using Periodic Perturbation Method and OPLS Force Field. *Fluid Phase Equilibria* **2007**, *260* (2), 212–217. https://doi.org/10.1016/j.fluid.2007.06.028.

(88) Sneha, E.; Revikumar, A.; singh, J. Y.; Thampi, A. D.; Rani, S. Viscosity Prediction of Pongamia Pinnata (Karanja) Oil by Molecular Dynamics Simulation Using GAFF and OPLS Force Field. *J. Mol. Graph. Model.* **2020**, *101*, 107764. https://doi.org/10.1016/j.jmgm.2020.107764.

(89) González, M. A.; Abascal, J. L. F. The Shear Viscosity of Rigid Water Models. *J. Chem. Phys.* **2010**, *132* (9), 096101. https://doi.org/10.1063/1.3330544.

(90) Ono, T.; Horikawa, K.; Maeda, Y.; Ota, M.; Sato, Y.; Inomata, H. Dynamic Properties of Methanol–Water Mixtures at the Temperatures up to 476.2 K and at High Pressures via Molecular Dynamics Simulation. *Fluid Phase Equilibria* **2016**, *420*, 30–35. https://doi.org/10.1016/j.fluid.2015.12.010.

(91) Yadav, A.; Trivedi, S.; Rai, R.; Pandey, S. Densities and Dynamic Viscosities of (Choline Chloride+glycerol) Deep Eutectic Solvent and Its Aqueous Mixtures in the Temperature Range (283.15–363.15)K. *Fluid Phase Equilibria* **2014**, *367*, 135–142. https://doi.org/10.1016/j.fluid.2014.01.028.

(92) Yadav, A.; Kar, J. R.; Verma, M.; Naqvi, S.; Pandey, S. Densities of Aqueous Mixtures of (Choline Chloride+ethylene Glycol) and (Choline Chloride+malonic Acid) Deep Eutectic Solvents in Temperature Range 283.15–363.15K. *Thermochim. Acta* **2015**, *600*, 95–101. https://doi.org/10.1016/j.tca.2014.11.028.

(93) Wu, S.-H.; Caparanga, A. R.; Leron, R. B.; Li, M.-H. Vapor Pressure of Aqueous Choline Chloride-Based Deep Eutectic Solvents (Ethaline, Glyceline, Maline and Reline) at 30–70°C. *Thermochim. Acta* **2012**, *544*, 1–5. https://doi.org/10.1016/j.tca.2012.05.031.

(94) Durand, E.; Lecomte, J.; Baréa, B.; Dubreucq, E.; Lortie, R.; Villeneuve, P. Evaluation of Deep Eutectic Solvent–Water Binary Mixtures for Lipase-Catalyzed Lipophilization of Phenolic Acids. *Green Chem.* **2013**, *15* (8), 2275. https://doi.org/10.1039/c3gc40899j.

(95) Wang, Y.; Ma, C.; Liu, C.; Lu, X.; Feng, X.; Ji, X. Thermodynamic Study of Choline Chloride-Based Deep Eutectic Solvents with Water and Methanol. *J. Chem. Eng. Data* **2020**, *65* (5), 2446–2457. https://doi.org/10.1021/acs.jced.9b01113.

(96) Abbott, A. P.; Harris, R. C.; Ryder, K. S.; D'Agostino, C.; Gladden, L. F.; Mantle, M. D. Glycerol Eutectics as Sustainable Solvent Systems. *Green Chem* **2011**, *13* (1), 82–90. https://doi.org/10.1039/C0GC00395F.

(97) Celebi, A. T.; Vlugt, T. J. H.; Moultos, O. A. Structural, Thermodynamic, and Transport Properties of Aqueous Reline and Ethaline Solutions from Molecular Dynamics Simulations. *J. Phys. Chem. B* **2019**, *123* (51), 11014–11025. https://doi.org/10.1021/acs.jpcb.9b09729.

(98) Jahn, D. A.; Akinkunmi, F. O.; Giovambattista, N. Effects of Temperature on the Properties of Glycerol: A Computer Simulation Study of Five Different Force Fields. *J. Phys. Chem. B* **2014**, *118* (38), 11284–11294. https://doi.org/10.1021/jp5059098.

(99) Caleman, C.; van Maaren, P. J.; Hong, M.; Hub, J. S.; Costa, L. T.; van der Spoel, D. Force Field Benchmark of Organic Liquids: Density, Enthalpy of Vaporization, Heat Capacities, Surface Tension, Isothermal Compressibility, Volumetric Expansion Coefficient, and Dielectric Constant. *J. Chem. Theory Comput.* **2012**, *8* (1), 61–74. https://doi.org/10.1021/ct200731v.

(100) Wagle, D. V.; Deakyne, C. A.; Baker, G. A. Quantum Chemical Insight into the Interactions and Thermodynamics Present in Choline Chloride Based Deep Eutectic Solvents. *J. Phys. Chem. B* **2016**, *120* (27), 6739–6746. https://doi.org/10/f8v6n4.

(101) Alizadeh, V.; Geller, D.; Malberg, F.; Sánchez, P.; Padua, A.; Kirchner, B. Strong Microheterogeneity in Novel Deep Eutectic Solvents. *ChemPhysChem* **2019**, *20*, 1786–1792. https://doi.org/10.1002/cphc.201900307.

(102) Kaur, S.; Gupta, A.; Kashyap, H. K. Nanoscale Spatial Heterogeneity in Deep Eutectic Solvents. *J. Phys. Chem. B* **2016**, *120* (27), 6712–6720. https://doi.org/10/f8v363.

(103) Kaur, S.; Kumari, M.; Kashyap, H. K. Microstructure of Deep Eutectic Solvents: Current Understanding and Challenges. *J. Phys. Chem. B* **2020**, *124* (47), 10601–10616. https://doi.org/10.1021/acs.jpcb.0c07934.

(104) Ma, C.; Laaksonen, A.; Liu, C.; Lu, X.; Ji, X. The Peculiar Effect of Water on Ionic Liquids and Deep Eutectic Solvents. *Chem. Soc. Rev.* **2018**, *47* (23), 8685–8720. https://doi.org/10.1039/C8CS00325D.

(105) Petrović, D.; Wang, X.; Strodel, B. How Accurately Do Force Fields Represent Protein Side Chain Ensembles? *Proteins Struct. Funct. Bioinforma.* **2018**, *86* (9), 935–944. https://doi.org/10.1002/prot.25525.

(106) Schröder, C.; Rudas, T.; Boresch, S.; Steinhauser, O. Simulation Studies of the Protein-Water Interface. I. Properties at the Molecular Resolution. *J. Chem. Phys.* **2006**, *124* (23), 234907. https://doi.org/10.1063/1.2198802.

For Table of Contents Only: